Angewandte Chemie
Eine Zeitschrift der Gesellschaft Deutscher Chemiker

Supporting Information

A Disilene Base Adduct with a Dative Si–Si Single Bond

Julia I. Schweizer, Markus G. Scheibel, Martin Diefenbach, Felix Neumeyer, Christian Würtele, Natalia Kulminskaya, Rasmus Linser, Norbert Auner, Sven Schneider, and Max C. Holthausen**

anie_201510477_sm_miscellaneous_information.pdf

(A) Experimental Section

All manipulations were carried out using standard Schlenk techniques in an inert nitrogen or argon atmosphere or in an argon-filled glove box. Solvents were dried by passing through columns packed with activated alumina. Deuterated solvents were dried over Na/K, distilled by trap-to-trap transfer in *vacuo* and degassed by three freeze-pump-thaw cycles. NMe_2Et was dried over CaH_2 and distilled prior to use. Si_2Cl_6 and *neo*-Si_5Cl_{12} were prepared according to published procedures.[1-3] Elemental analyses were obtained from the analytical laboratories at Göttingen University on an Elementar Vario EL 3. Solution NMR spectra were recorded on a Bruker Avance III 400 MHz spectrometer and were calibrated to the residual solvent proton resonance ([D_6]benzene: δ_H = 7.16 ppm; [D_8]toluene: δ_H = 2.09 ppm). ^{29}Si chemical shifts are reported relative to external tetramethylsilane (δ = 0 ppm). Solid-state NMR spectra were recorded on a Bruker Avance III 400 MHz spectrometer, equipped with a standard 4 mm triple-resonance magic-angle spinning (MAS) probe. ^{1}H-^{29}Si cross-polarization (CP) spectra shown were recorded using an MAS frequency of 11 kHz, 12 ms acquisition time with 85 kHz SPINAL-64 proton decoupling and 8 ms CP contact time (unless otherwise indicated) with ^{1}H and ^{29}Si B_1 fields of 60 and 70 kHz, respectively, using a 80-100% ramp on proton. All experiments were acquired with a sample temperature of 5 °C and using a spectral width of 1258 ppm, 3s repetition delay and a number of scans of 1k for each spectrum. All spectra were referenced relative to an external TMS sample and apodized using 50 Hz exponential multiplication. Raman spectra were recorded using a HORIBA Scientific LabRAM HR 800 (400-1100 nm) spectrometer with open-electrode CCD detector and a confocal pinhole with user controlled variable aperture in combination with a free space optical microscope and a He:Ne-laser (632.8 nm).

A1. Synthesis of $EtMe_2N(Cl)_2SiSi(SiCl_3)_2$ (1) from Si_2Cl_6

NMe_2Et (300 µL, 2.9 mmol, 1 eq.) was added to a solution of Si_2Cl_6 (500 µL, 2.9 mmol, 1 eq.) in benzene (1 mL) at room temperature (RT). The resulting yellow solution was subsequently cooled to −196 °C. After one hour, the mixture was thawed to RT to yield colorless crystals in a yellow solution. The solvent was then filtered off and the residue was washed with cold pentane (2 x 3mL). The isolated product was dried under vacuum to give colorless **1** (257 mg, 0.6 mmol, 83%). Sample preparation for spectroscopic characterization in solution was performed at temperatures strictly below -50°C. ^{1}H NMR (400 MHz, [D_8]toluene, 223 K): δ = 2.35 (q, ^3J(H,H) = 6.7 Hz, 2 H, NCH_2), 1.58 (s, 6 H, NCH_3), 0.15 (t, ^3J(H,H) = 6.7 Hz, 3 H, NCH_2CH_3) ppm. ^{29}Si{^{1}H} NMR (79.5 MHz, [D_8]toluene, 243 K): δ = 43.7 (s, 1 Si, $EtMe_2N$-*Si*Cl_2), 27.9 (s, 2 Si, Si(*Si*Cl_3)$_2$), −155.6 (s, 1 Si, *Si*($SiCl_3$)$_2$) ppm. ^{29}Si CP/MAS NMR (79.5 MHz, 243 K): δ = 43.7 (s, 1 Si, $EtMe_2N$-*Si*Cl_2), 27.9 (s, 2 Si, Si(*Si*Cl_3)$_2$), −155.6 (s, 1 Si, *Si*($SiCl_3$)$_2$) ppm. Slow proton-silicon magnetization transfer behavior characterized by CP buildup experiments confirmed the absence of directly bonded protons for all Si sites (cf. Figure S3). NMR assignments are based on relativistic spin-orbit DFT calculations for Si (cf. section C4) and were confirmed by ^{1}H-^{29}Si HMBC spectroscopy in solution (cf. Figure S4). Anal. Calc. for $C_4H_{11}Cl_8NSi_4$ (469.08): C 10.24, H 2.36, N 2.99; found C 10.97, H 2.40, N 2.48; the deviation is consistent with the presence of minor amounts of co-crystallized benzene as detected by ^{1}H NMR spectroscopy. Raman-spectroscopic data of solid **1** fits well to the calculated spectrum (Figure S5).

A2. Synthesis of $EtMe_2N(Cl)_2SiSi(SiCl_3)_2$ (1) from *neo*-Si_5Cl_{12}

NMe_2Et (28.7 µL, 0.3 mmol, 1 eq.) was added to a suspension of *neo*-Si_5Cl_{12} (150 mg, 0.3 mmol, 1 eq.) in [D_8]toluene (370 µL) in a J-Young NMR tube at –196 °C by trap-to-trap condensation. The mixture was warmed to –70 °C and immediately examined *in situ* by NMR spectroscopy. $^{29}Si\{^1H\}$ (400 MHz, [D_8]toluene, 203 K): δ = 43.7 (s, 1 Si, $EtMe_2N$-*Si*Cl_2), 29.4 (s, 2 Si, Si(*Si*$Cl_3)_2$), –158.3 (s, 1 Si, *Si*$(SiCl_3)_2$); –18.5 (*Si*Cl_4); 30.9 (s, [Si(*Si*$Cl_3)_3]^-$), –68.8 (s, [$(Me_3N)_2$*Si*$Cl_3]^+$), –143.1 (s, [*Si*$(SiCl_3)_3]^-$) ppm.

A3. Crystallization of $EtMe_2N(Cl)_2SiSi(SiCl_3)_2$ (1) from benzene

NMe_2Et (59.2 µL, 0.58 mmol, 1 eq.) was added to a solution of Si_2Cl_6 (100 µL, 0.58 mmol, 1 eq.) in benzene (340 µL). The resulting yellow solution was subsequently cooled to –196 °C and kept at this temperature for 20 minutes**.** Upon thawing to RT, single crystals suitable for X-ray diffraction analysis precipitated and were isolated from the mother liquor.

A4. Crystallization of $EtMe_2N(Cl)_2SiSi(SiCl_3)_2$ (1) from toluene

NMe_2Et (59.2 µL, 0.58 mmol, 1 eq.) was added to a solution of Si_2Cl_6 (100 µL, 0.58 mmol, 1 eq.) in [D_8]toluene (340 µL). The resulting yellow solution was subsequently cooled to –196 °C. After thawing the reaction was monitored by variable temperature NMR spectroscopy at 193 K, 203 K, 223 K and 263 K (30 minutes each). The reaction mixture was then warmed to RT. Single crystals suitable for X-ray diffraction were isolated from the mother liquor.

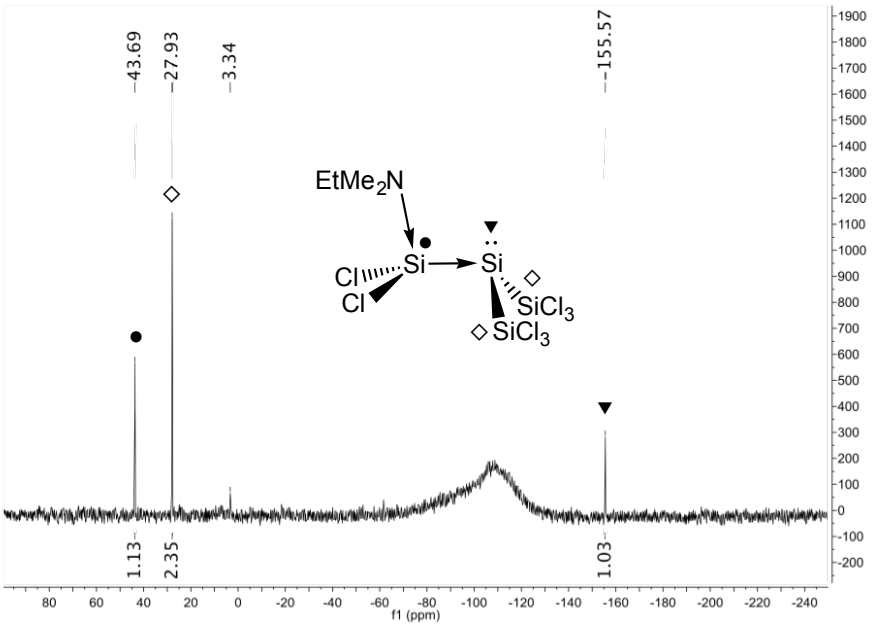

Figure S1. $^{29}Si\{^1H\}$ NMR spectrum of compound **1** at 243K in [D_8]toluene.

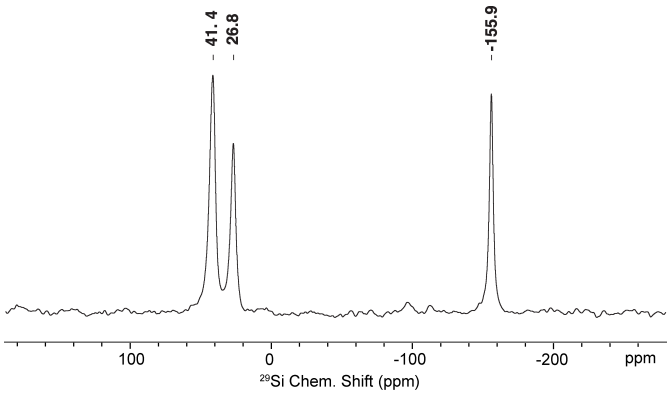

Figure S2. ^{29}Si CP NMR spectrum of compound **1** at 5 °C, acquired using magic angle spinning (MAS) of 11 kHz. The ^{1}H-^{29}Si CP contact time was set to 8 ms. rf fields were set to 60 kHz and 70 kHz on ^{1}H and ^{29}Si, respectively. 12 ms acquisition time was used in the experiment upon 85 kHz SPINAL-64 proton decoupling.

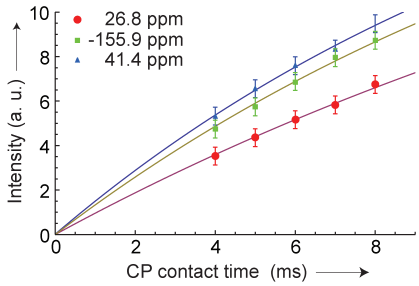

Figure S3. CP build-up curve for ^{1}H/^{29}Si magnetization transfer at 11 kHz MAS, showing the signal intensity dependent on the cross-polarization contact time. The slow increase of signal intensity not reaching a maximum even after 8 ms shows the absence of directly bonded protons at the Si centers. This is true for all three positions, having very similar buildup behavior.

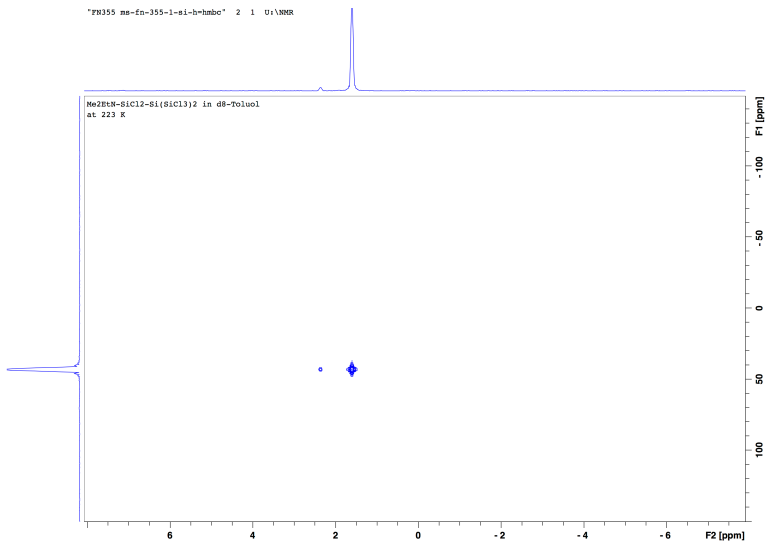

Figure S4. ^{1}H-^{29}Si-HMBC-NMR spectrum of compound **1** in [D$_8$]toluene at –50 ºC.

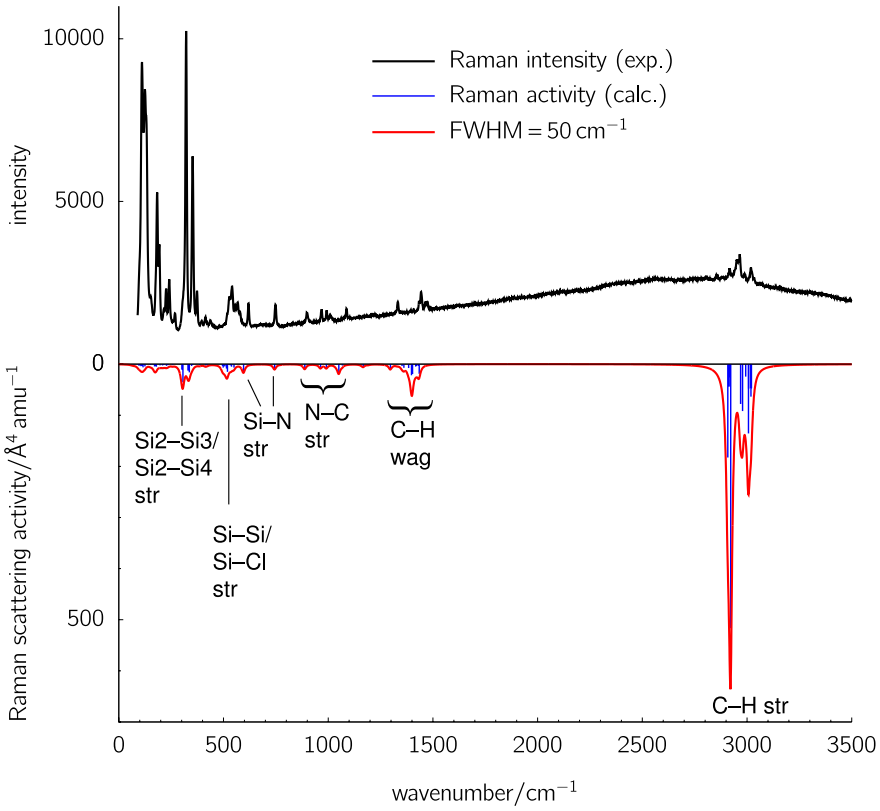

Figure S5. Experimental (top) and computed (bottom) Raman spectrum of **1**. Computed harmonic frequencies (SMD-M06-2X/6-31+G(d,p), solvent toluene) were corrected by a fundamental frequency scale factor of 0.940.[4]

(B) Crystallographic Details

CCDC-1433842 (**1**·C_6D_6) and CCDC-1433843 (**1**) contain the supplementary crystallographic data for this paper. This data can be obtained free of charge via http://www.ccdc.cam.ac.uk/products/csd/request/ (or from Cambridge Crystallographic Data Centre, 12 Union Road, Cambridge, CB2 1EZ, UK. Fax: +44-1223- 336-033; e-mail: deposit@ccdc.cam.ac.uk).

Suitable single crystals for X-ray structure determination were selected from the mother liquor under an inert gas atmosphere and transferred in protective perfluoro polyether oil on a microscope slide. The selected and mounted crystals were transferred to the cold gas stream on the diffractometer. Intensity data for **1**·C_6D_6 and **1** were obtained at 100 K on a Bruker D8 three-circle diffractometer, equipped with a PHOTON 100 CMOS detector and an INCOATEC microfocus source with Quazar mirror optics (λ= 0.71073 Å). The data obtained were integrated with SAINT and a multi-scan absorption correction with SADABS was applied. Both structures were solved and refined using the Bruker SHELX 2014 software package.[5]

All non-hydrogen atoms were refined with anisotropic displacement parameters. All C-H hydrogen atoms were refined isotropically on calculated positions by using a riding model with their U_{iso} values constrained to 1.5 U_{eq} of their pivot atoms for terminal sp^3 carbon atoms and 1.2 times for all other carbon atoms.

B1. X-ray Single-Crystal Structure Analysis of 1 from Benzene

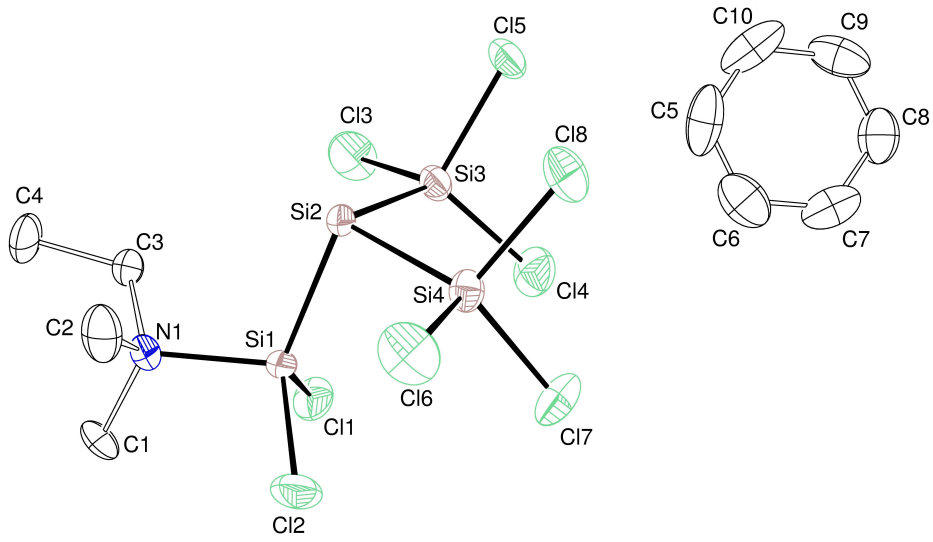

Figure S6. Molecular structure of **1**. Ellipsoids shown at 50% probability. Hydrogen atoms omitted for clarity.

Table S1. Crystal data and structure refinement for **1**·C_6D_6.

Identification code	CW_MS_MH_020215	
Empirical formula	$C_{10}H_{11}Cl_8D_6NSi_4$	
Formula weight	553.24	
Temperature	173(2) K	
Wavelength	0.71073 Å	
Crystal system	Orthorhombic	
Space group	$P2_12_12_1$	
Unit cell dimensions	a = 10.6497(4) Å	α = 90°
	b = 12.5486(4) Å	β = 90°
	c = 17.5895(7) Å	γ = 90°
Volume	2350.64(15) Å^3	
Z	4	
Density (calculated)	1.563 Mg/m^3	
Absorption coefficient	1.159 mm^{-1}	
F(000)	1104	
Crystal size	0.234 x 0.162 x 0.072 mm^3	
Theta range for data collection	2.236 to 27.195°	
Index ranges	-13<=h<=13, -16<=k<=16, -22<=l<=22	
Reflections collected	29456	
Independent reflections	5189 [R(int) = 0.0392]	
Completeness to theta = 25.242°	100.0 %	
Absorption correction	Semi-empirical from equivalents	
Max. and min. transmission	0.7455 and 0.6193	
Refinement method	Full-matrix least-squares on F^2	
Data / restraints / parameters	5189 / 0 / 211	
Goodness-of-fit on F^2	1.358	
Final R indices [I>2sigma(I)]	R1 = 0.0477	wR2 = 0.0925
R indices (all data)	R1 = 0.0515	wR2 = 0.0941
Absolute structure parameter	0.03(2)	
Largest diff. peak and hole	0.384 and -0.393 eÅ^{-3}	

Table S2. Bond lengths [Å] and angles [°] for **1**·C_6D_6.

C(1)-N(1)	1.504(7)	C(9)-C(10)-C(5)	119.5(8)
C(2)-N(1)	1.503(8)	C(2)-N(1)-C(1)	109.2(5)
C(3)-C(4)	1.511(7)	C(2)-N(1)-C(3)	109.8(5)
C(3)-N(1)	1.526(7)	C(1)-N(1)-C(3)	110.3(5)
C(5)-C(6)	1.345(12)	C(2)-N(1)-Si(1)	107.6(4)
C(5)-C(10)	1.377(13)	C(1)-N(1)-Si(1)	112.8(4)
C(6)-C(7)	1.353(11)	C(3)-N(1)-Si(1)	107.2(3)
C(7)-C(8)	1.356(11)	N(1)-Si(1)-Cl(2)	101.80(17)
C(8)-C(9)	1.349(12)	N(1)-Si(1)-Cl(1)	101.13(17)
C(9)-C(10)	1.362(12)	Cl(2)-Si(1)-Cl(1)	105.82(10)
N(1)-Si(1)	1.894(5)	N(1)-Si(1)-Si(2)	107.14(15)
Si(1)-Cl(2)	2.037(2)	Cl(2)-Si(1)-Si(2)	116.76(10)
Si(1)-Cl(1)	2.045(2)	Cl(1)-Si(1)-Si(2)	121.32(9)
Si(1)-Si(2)	2.324(2)	Si(3)-Si(2)-Si(4)	97.46(8)
Si(2)-Si(3)	2.310(2)	Si(3)-Si(2)-Si(1)	96.90(8)
Si(2)-Si(4)	2.317(2)	Si(4)-Si(2)-Si(1)	96.93(8)

Si(3)-Cl(3)	2.047(2)	Cl(3)-Si(3)-Cl(4)	105.98(11)
Si(3)-Cl(4)	2.053(2)	Cl(3)-Si(3)-Cl(5)	105.23(10)
Si(3)-Cl(5)	2.057(2)	Cl(4)-Si(3)-Cl(5)	104.44(10)
Si(4)-Cl(6)	2.046(2)	Cl(3)-Si(3)-Si(2)	109.50(9)
Si(4)-Cl(7)	2.048(2)	Cl(4)-Si(3)-Si(2)	121.82(9)
Si(4)-Cl(8)	2.065(2)	Cl(5)-Si(3)-Si(2)	108.64(10)
C(4)-C(3)-N(1)	115.4(5)	Cl(6)-Si(4)-Cl(7)	104.85(11)
C(6)-C(5)-C(10)	120.2(8)	Cl(6)-Si(4)-Cl(8)	104.55(10)
C(5)-C(6)-C(7)	119.2(8)	Cl(7)-Si(4)-Cl(8)	104.74(10)
C(6)-C(7)-C(8)	121.7(7)	Cl(6)-Si(4)-Si(2)	110.89(10)
C(9)-C(8)-C(7)	119.2(8)	Cl(7)-Si(4)-Si(2)	122.22(9)
C(8)-C(9)-C(10)	120.3(8)	Cl(8)-Si(4)-Si(2)	108.15(9)

Table S3. Torsion angles [°] for **1**·C_6D_6.

C(10)-C(5)-C(6)-C(7)	0.0(12)	C(2)-N(1)-Si(1)-Cl(2)	65.9(4)
C(5)-C(6)-C(7)-C(8)	0.5(12)	C(1)-N(1)-Si(1)-Cl(2)	-54.6(5)
C(6)-C(7)-C(8)-C(9)	-0.5(12)	C(3)-N(1)-Si(1)-Cl(2)	-176.1(3)
C(7)-C(8)-C(9)-C(10)	0.1(12)	C(2)-N(1)-Si(1)-Cl(1)	174.8(4)
C(8)-C(9)-C(10)-C(5)	0.3(12)	C(1)-N(1)-Si(1)-Cl(1)	54.4(5)
C(6)-C(5)-C(10)-C(9)	-0.4(12)	C(3)-N(1)-Si(1)-Cl(1)	-67.2(3)
C(4)-C(3)-N(1)-C(2)	-55.5(6)	C(2)-N(1)-Si(1)-Si(2)	-57.2(4)
C(4)-C(3)-N(1)-C(1)	64.8(6)	C(1)-N(1)-Si(1)-Si(2)	-177.7(4)
C(4)-C(3)-N(1)-Si(1)	-172.1(4)	C(3)-N(1)-Si(1)-Si(2)	60.8(4)

B2. X-ray Single-Crystal Structure Analysis of 1 from Toluene

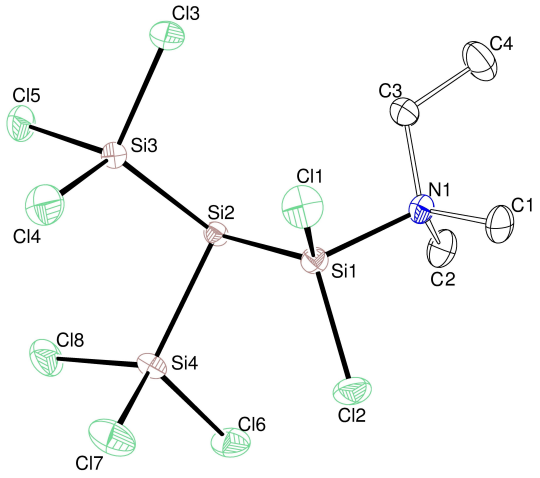

Figure S7. Molecular structure of **1**. Ellipsoids shown at 50% probability. Hydrogen atoms omitted for clarity.

Table S4. Crystal data and structure refinement for **1.**

Identification code	CW_MS_MH_050215_2_a	
Empirical formula	$C_4H_{11}Cl_8NSi_4$	
Formula weight	469.10	
Temperature	173(2) K	
Wavelength	0.71073 Å	
Crystal system	Monoclinic	
Space group	$P2_1/c$	
Unit cell dimensions	a = 14.2065(7) Å	α = 90°
	b = 10.4878(5) Å	β = 104.284(2)°
	c = 12.7589(7) Å	γ = 90°
Volume	1842.24(16) Å3	
Z	4	
Density (calculated)	1.691 Mg/m^3	
Absorption coefficient	1.463 mm^{-1}	
F(000)	936	
Crystal size	0.283 x 0.145 x 0.128 mm^3	
Theta range for data collection	2.441 to 30.596°	
Index ranges	-20<=h<=20, -15<=k<=14, -18<=l<=18	
Reflections collected	88887	
Independent reflections	5663 [R(int) = 0.0642]	
Completeness to theta = 25.242°	100.0 %	
Absorption correction	Semi-empirical from equivalents	
Max. and min. transmission	0.7461 and 0.6779	
Refinement method	Full-matrix least-squares on F^2	
Data / restraints / parameters	5663 / 0 / 157	
Goodness-of-fit on F^2	1.083	
Final R indices [I>2sigma(I)]	R1 = 0.0311	wR2 = 0.0510
R indices (all data)	R1 = 0.0543	wR2 = 0.0566
Largest diff. peak and hole	0.450 and -0.491 $eÅ^{-3}$	

Table S5. Bond lengths [Å] and angles [°] for **1.**

C(1)-N(1)	1.506(2)	C(3)-N(1)-Si(1)	106.79(9)
C(2)-N(1)	1.505(2)	N(1)-Si(1)-Cl(2)	100.86(4)
C(3)-C(4)	1.512(2)	N(1)-Si(1)-Cl(1)	100.86(5)
C(3)-N(1)	1.522(2)	Cl(2)-Si(1)-Cl(1)	105.79(3)
N(1)-Si(1)	1.9014(13)	N(1)-Si(1)-Si(2)	106.98(4)
Si(1)-Cl(2)	2.0482(6)	Cl(2)-Si(1)-Si(2)	116.12(2)
Si(1)-Cl(1)	2.0509(6)	Cl(1)-Si(1)-Si(2)	122.92(3)
Si(1)-Si(2)	2.3225(6)	Si(3)-Si(2)-Si(4)	99.22(2)
Si(2)-Si(3)	2.3090(6)	Si(3)-Si(2)-Si(1)	97.63(2)
Si(2)-Si(4)	2.3190(6)	Si(4)-Si(2)-Si(1)	96.40(2)
Si(3)-Cl(3)	2.0546(6)	Cl(3)-Si(3)-Cl(4)	105.90(3)
Si(3)-Cl(4)	2.0548(6)	Cl(3)-Si(3)-Cl(5)	104.63(3)
Si(3)-Cl(5)	2.0551(6)	Cl(4)-Si(3)-Cl(5)	104.94(3)
Si(4)-Cl(7)	2.0514(6)	Cl(3)-Si(3)-Si(2)	109.42(2)
Si(4)-Cl(6)	2.0519(6)	Cl(4)-Si(3)-Si(2)	122.02(3)
Si(4)-Cl(8)	2.0606(6)	Cl(5)-Si(3)-Si(2)	108.59(3)
C(4)-C(3)-N(1)	115.42(14)	Cl(7)-Si(4)-Cl(6)	105.09(3)
C(1)-N(1)-C(2)	108.63(12)	Cl(7)-Si(4)-Cl(8)	103.66(3)
C(1)-N(1)-C(3)	110.23(13)	Cl(6)-Si(4)-Cl(8)	106.48(3)
C(2)-N(1)-C(3)	110.18(13)	Cl(7)-Si(4)-Si(2)	124.35(3)
C(1)-N(1)-Si(1)	108.37(10)	Cl(6)-Si(4)-Si(2)	106.87(2)
C(2)-N(1)-Si(1)	112.62(10)	Cl(8)-Si(4)-Si(2)	109.19(3)

Table S6. Torsion angles [°] for **1**.

C(4)-C(3)-N(1)-C(1)	57.77(19)
C(4)-C(3)-N(1)-C(2)	-62.10(19)
C(4)-C(3)-N(1)-Si(1)	-179.59(13)

(C) Quantum-Chemical Section

All geometry optimizations and harmonic frequency calculations have been conducted using the Gaussian09 program package[6] employing the M06-2X density functional[7] in combination with the 6-31+G(d,p) split-valence basis set[8]. The SMD polarizable continuum model[9] was employed to account for solvent effects (toluene). To avoid the occurrence of spurious imaginary modes due to integration grid errors, the 'ultrafine' grid option was used throughout for numerical integrations.[10] Stationary points were characterized as minima or first order saddle points by eigenvalue analysis of the computed Hessians. Connectivities between minima and transition states implied in figures and schemes were validated either by intrinsic-reaction-coordinate (IRC) following calculations or by displacing the transition state geometries along both directions of the transition mode, followed by unconstrained optimizations to the respective minima. Single-point calculations were conducted on the optimized geometries using the M06-2X functional in combination with the 6-311++G(2d,2p) basis set;[11-12] also the wave functions used for bonding analysis were obtained at this level of theory, dubbed SMD-M06-2X/6-311++G(2d,2p)//6-31+G(d,p). Natural bond orbital (NBO) and natural resonance theory (NRT) analyses were performed using the NBO 6.0 program[13] interfaced with the Gaussian09 program.[14-15] The Multiwfn program[16-17] was used for QTAIM analyses[18-19]. Unscaled zero-point vibrational energies as well as thermal and entropic correction terms were obtained from Hessian matrices computed at the M06-2X/6-31+G(d,p) level using standard procedures as implemented in Gaussian09 and were used to obtain Gibbs Free energies at 203.15 K. ΔG_{203} is given in kcal mol^{-1}.

The choice of the basis set evidently plays a crucial role in terms of the computed wavefunction and the resulting topological analysis of the electron density in silicon-bonded molecules, as has also been pointed out earlier by Zhikol and colleagues.[20] The topology of the electron density is especially prone to the appearance of non-nuclear attractors (NNAs or *pseudo-atoms* along the Si–Si bond between the two silicon nuclei), which are caused by basis-set inadequacies only, and are therefore considered unphysical. Zhikol and coworkers have traced back this phenomenon to an inadequate representation of the radial extent of the s, p, and d shells, and they recommend Pople-style basis sets with two d-polarization functions on Si. Correspondingly, we chose the 6-311++G(2d,2p) basis set for the analysis of wavefunctions.

Based on geometries optimized at the SMD-M06-2X/6-31+G(d,p) level, NMR chemical shift values were calculated with the NMR module[21-22] of the ADF program.[23-24] Relativistic spin-orbit contributions to nuclear magnetic shielding constants were accounted for by means of the two-component zeroth-order regular approximation (ZORA) formalism implemented in ADF.[25-28] The PBE0 hybrid functional[29-31] was employed in combination with the triple-ζ Slater-type basis set (TZ2P).[32] ^{29}Si NMR chemical shifts are reported relative to tetramethylsilane (δ^{29}Si(TMS) = 0). Solvent effects were taken into account with the conductor-like screening model (COSMO) implemented in ADF (toluene, dielectric constant ε = 2.38, solvent radius = 3.48 Å).[33-34] Energy decomposition analysis with natural orbitals for chemical valence (EDA-NOCV)[35-36] has been performed with ADF, employing the BP86-D/TZ2P level of theory (gas phase calculations) on SMD-M06-2X/6-31+G(d,p) structures.

Pictures of molecular structures were generated with the Cylview[37] and ChemCraft[38] programs.

C1. NBO Analyses of 1 and 2

Table S7. Selected results of the NBO and NRT analyses of **1**; wave functions computed at the SMD-M06-2X/6-311++G(2d,2p)//6-31+G(d,p) level of DFT (solvent toluene).

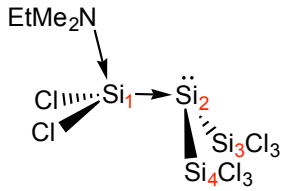

Bond	NBO analysis (NLMOs)[a]			NRT analysis[b]	
	pol. [%]	hybr.	WBI	bond	tot/cov/ionic
N1–Si1	86% (N1)	$sp^{3.71}$(N1)	0.34	N1–Si1	0.56/0.13/0.43
	12% (Si1)	$sp^{2.05}$(Si1)			
Si1–Si2	57% (Si1)	$sp^{0.63}$(Si1)	1.03	Si1–Si2	1.01/0.77/0.24
	40% (Si2)	$sp^{5.99}$(Si2)			
Si2–Si3	41% (Si2)	$sp^{5.74}$(Si2)	0.94	Si2–Si3	0.95/0.80/0.15
	55% (Si3)	$sp^{0.83}$(Si3)			
Si2–Si4	41% (Si2)	$sp^{6.16}$(Si2)	0.94	Si2–Si4	0.95/0.79/0.16
	55% (Si4)	$sp^{0.86}$(Si4)			

[a] pol. = polarization, hybr. = hybridization, WBI = Wiberg bond index.
[b] Natural bond order (tot/cov/ionic: total/covalent/ionic).

Table S8. Fragment charges obtained from NPA analysis of **1**; wave functions computed at the SMD-M06-2X/6-311++G(2d,2p)//6-31+G(d,p) level of DFT (solvent toluene).

Fragment	NPA charge/e
NMe_2Et	0.24
$SiCl_2$	0.45
$Si(SiCl_3)_2$	–0.69

Table S9. Selected results of the NBO and NRT analyses of **2**; wave functions computed at the SMD-M06-2X/6-311++G(2d,2p)//6-31+G(d,p) level of DFT (solvent toluene).

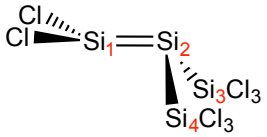

Bond	NBO analysis (NLMOs)[a]			NRT analysis[b]	
	pol. [%]	hybr.	WBI	bond	tot/cov/ionic
σ(Si1–Si2)	55% (Si1)	$sp^{0.55}$(Si1)	1.30	Si1–Si2	1.38/0.95/0.43
	43% (Si2)	$sp^{1.41}$(Si2)			
π(Si1–Si2)	24% (Si1)	$sp^{2.53}$(Si1)			
	69% (Si2)	$sp^{1.98}$(Si2)			
Si2–Si3	46% (Si2)	$sp^{1.87}$(Si2)	0.91	Si2–Si3	0.93/0.84/0.08
	51% (Si3)	$sp^{1.08}$(Si3)			
Si2–Si4	46% (Si2)	$sp^{2.05}$(Si2)	0.91	Si2–Si4	0.93/0.83/0.09
	51% (Si4)	$sp^{1.06}$(Si4)			

[a] pol. = polarization, hybr. = hybridization, WBI = Wiberg bond index.
[b] tot/cov/ionic: total/covalent/ionic bond order.

Table S10. Fragment charges obtained from NPA analysis of **2**; wave functions computed at the SMD-M06-2X/6-311++G(2d,2p)//6-31+G(d,p) level of DFT (solvent toluene).

Fragment	NPA charge/e
$SiCl_2$	0.40
$Si(SiCl_3)_2$	–0.40

C2. QTAIM Analyses of 1 and 2

Table S11. Selected properties of the electron density distribution in **1** and **2**; atom numbering as in the X-ray structure displayed in Figure S6. Bond path lengths $d_{A–B}$, and distances to bcps $d_{A–bcp}$ and $d_{B–bcp}$ are given in Å, the electron density ρ_{bcp} in eÅ^{-3}, the Laplacian of the electron density $\nabla^2\rho_{bcp}$ in eÅ^{-5}, the total energy density H_{bcp} in E_hÅ^{-3}. $\varepsilon_{bcp} = \lambda_1/\lambda_2 - 1$ is the bond ellipticity derived from the two negative eigenvalues of the Hessian matrix of the electron density at the bcp, with $\lambda_1 \geq \lambda_2$. The delocalization index $\delta_{A,B}$ represents the number of electron pairs (or total Fermi correlation) shared between two atoms. Atomic partial charges q_i (in e) from integration of the electron density over the corresponding atomic basins.

	$d_{A–B}$	$d_{A–bcp}$	$d_{B–bcp}$	ρ_{bcp}	$\nabla^2\rho_{bcp}$	H_{bcp}	ε_{bcp}	$\delta_{A,B}$	q_A	q_B
1										
N1–Si1	1.89	1.16	0.73	0.63	4.36	−0.34	0.05	0.40	−1.18	1.68
Si1–Si2	2.30	1.41	0.89	0.54	−1.86	−0.31	0.13	0.79	1.68	0.50
Si2–Si3	2.32	0.95	1.37	0.56	−2.53	−0.29	0.09	0.78	0.50	1.79
Si2–Si4	2.32	0.97	1.35	0.56	−2.56	−0.29	0.09	0.78	0.50	1.82
Si1–Cl1	2.04	0.75	1.29	0.65	3.28	−0.39	0.05	0.57	1.68	−0.73
Si3–Cl3	2.05	0.75	1.30	0.63	2.98	−0.37	0.05	0.56	1.79	−0.75
2										
Si1–Si2	2.22	1.35	0.87	0.56	−1.70	−0.33	0.29	1.06	1.37	0.45
Si2–Si3	2.32	1.05	1.27	0.58	−2.76	−0.27	0.07	0.78	0.45	1.96
Si2–Si4	2.30	1.03	1.27	0.58	−2.69	−0.27	0.06	0.77	0.45	1.97
Si1–Cl1	1.98	0.73	1.25	0.71	4.12	−0.44	0.04	0.71	1.37	−0.69
Si3–Cl3	2.02	0.73	1.29	0.67	3.47	−0.41	0.04	0.57	1.97	−0.73

C3. EDA-NOCV calculations for 1 and 2

The nature of the N1–Si1 and Si1–Si2 bonding in **1** and **2** may be characterized in terms of their interacting fragments. Two types of bonding arise from a covalent interaction as a natural and obvious distinction, either formed from their corresponding open-shell radical bonding partners or from the complementary closed-shell donor–acceptor interactions. By applying the two different fragmentation schemes to the N1–Si1 bond, a donor–acceptor interaction is due to the two neutral closed-shell fragments, that is, a donor base fragment NMe_2Et carrying an electron lone pair and a disilene fragment **2** with an empty acceptor orbital. The associated fragments for symmetric electron sharing from two radical species are the respective radical ions $NMe_2Et^{+\bullet}$ and $\mathbf{2}^{-\bullet}$. Similarly, the Si1–Si2 bond in **1** may be described via heterolysis into a $EtMe_2N{\bullet}SiCl_2$ donor and the silylene acceptor $Si(SiCl_3)_2$, or via homolysis into the corresponding radical ion species. Table S12 below shows the energy decomposition analysis for both bonds in **1**. The best choice for the interacting fragments is given by the smallest $|\Delta E_{orb}|$ term, so that a minimal reorganization of the electronic structure is required. In both bonds, the donor–acceptor interaction is clearly favored with absolute ΔE_{orb} values of −106 and −118 kcal mol^{-1} for N1–Si1 and Si1–Si2, respectively, while those for the radical ion fragments amount to −207 and −136 kcal mol^{-1}. For each bond one major term ΔE_1 contributes to the orbital interaction after a breakdown into pairwise NOCV contributions. They are readily identified by their corresponding deformation densities $\Delta\rho_1$ (Figure S8, top) that arise from the HOMO–LUMO interactions of the corresponding fragments (Figure S8, bottom).

Notably, an identical picture emerges from fragmentation of **1** into the central ambiphilic $SiCl_2$ group and the "push-pull" stabilizing framework of a $Me_2EtN{\cdots}Si(SiCl_3)_2$ fragment, see Table S13 and Figure S9. Both, heterolysis and homolysis are now based on neutral fragments. In the closed-shell scheme each fragment provides an electron lone-pair and an acceptor orbital, while the open-shell radical bonding pattern is based on the two corresponding triplet fragments, where the former filled lone-pair and empty acceptor orbitals are singly occupied.

In analogy to the Si1–Si2 bond in **1**, the optimal fragmentation pattern into the neutral closed-shell donor and acceptor fragments $SiCl_2$ and $Si(SiCl_3)_2$ applies also to compound **2**, and the affiliated ΔE_{orb} value of −117 kcal mol^{-1} is clearly preferred over ΔE_{orb} = −183 kcal mol^{-1} for the charged doublet fragments $SiCl_2^{+\bullet}$ and $Si(SiCl_3)_2^{-\bullet}$, see Table S14. There are now two dominant pairwise orbital interaction contributions for the Si1–Si2 bond. One major term ΔE_1 accounts for 61 % of ΔE_{orb} and describes the Si1→Si2 σ-donation, and one smaller term ΔE_2 provides 29 % of ΔE_{orb}, arising from Si1←Si2 π-backdonation (see deformation densities $\Delta\rho_{1,2}$ and HOMO–LUMO plots in Figure S10).

Table S12. Energy decomposition analysis of **1** for the bonding in N1–Si1 and Si1–Si2 computed for neutral closed-shell singlet fragments and for charged doublet fragments (BP86-D/TZ2P//SMD-M06-2X/6-31+G(d,p)). Relative energies are given in kcal mol^{-1}.

Interaction	N1→Si1		N1··Si1		Si1→Si2		Si1··Si2	
ΔE_{int}	−62.5		−172.2		−75.1		−159.7	
ΔE_{disp}	−11.9		−11.9		−14.1		−14.1	
ΔE_{pauli}	187.2		232.6		168.0		153.6	
ΔE_{elstat} [a]	−131.4	(55.2 %)	−186.3	(47.4 %)	−111.1	(48.5 %)	−163.2	(54.5 %)
ΔE_{orb} [a]	−106.5	(44.8 %)	−206.7	(52.6 %)	−118.0	(51.5 %)	−136.0	(45.5 %)
ΔE_1 [b]	−77.7	(72.9 %)	−181.3	(87.7 %)	−92.8	(78.7 %)	−99.8	(73.4 %)

[a] The values in parentheses are relative to the attractive interactions $\Delta E_{\text{elstat}} + \Delta E_{\text{orb}}$.
[b] The values in parentheses are relative to the total orbital interactions ΔE_{orb}.

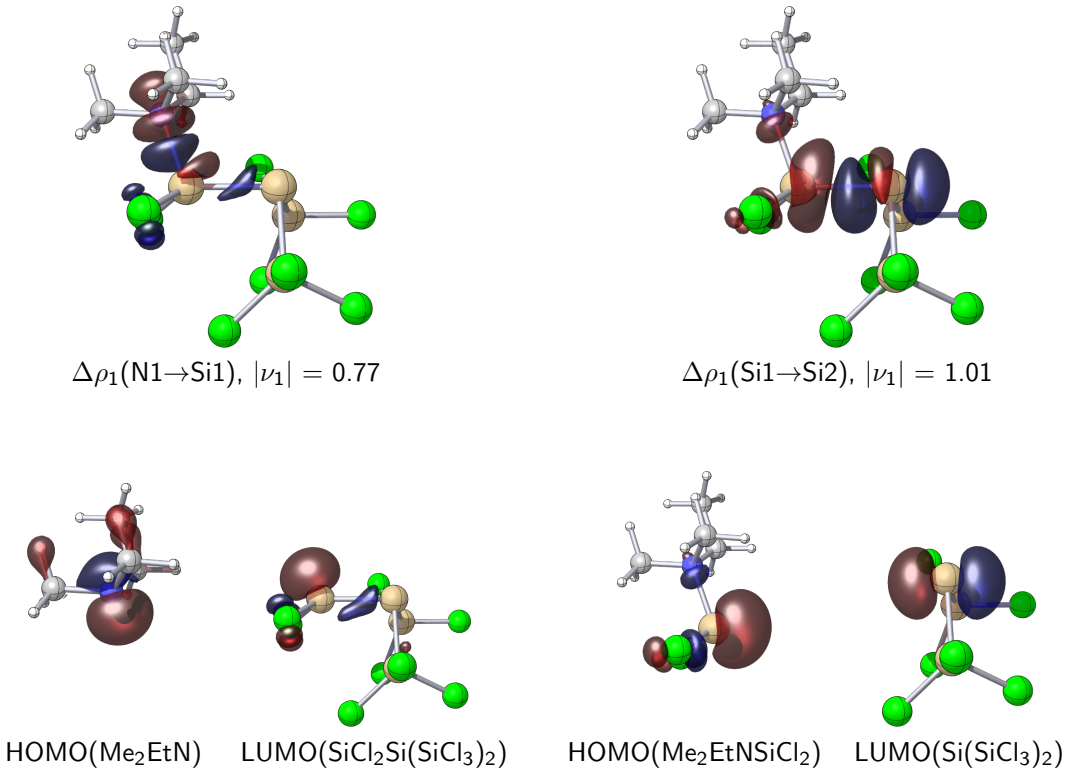

Figure S8. Deformation densities $\Delta\rho$ (isocontour 0.005 a_0^{-3}) from EDA-NOCV calculations on neutral closed-shell singlet fragments of **1**: N1–Si1 interaction (left) and Si1–Si2 interaction (right). The charge eigenvalues ν quantify the charge transfer between donor and acceptor fragments (in e). The corresponding frontier orbitals (isocontour 0.075 $a_0^{-3/2}$) of the fragments are shown (bottom).

Table S13. Energy decomposition analysis of **1** for the N1–Si1–Si2 bonding, relative to the ambiphilic $SiCl_2$ fragment and the embracing donor-acceptor fragment $Me_2EtN\cdots Si(SiCl_3)_2$ (BP86-D/TZ2P//SMD-M06-2X/6-31+G(d,p)). Relative energies are given in kcal mol^{-1}.

Interaction	D/A (N1→Si1→Si2)		shared (N1··Si1··Si2)	
ΔE_{int}	−87.5		−199.1	
ΔE_{disp}	−16.4		−16.4	
ΔE_{pauli}	385.3		363.2	
ΔE_{elstat}[a]	−196.6	(43.1 %)	−228.2	(41.8 %)
ΔE_{orb}[a]	−259.8	(56.9 %)	−317.7	(58.2 %)
ΔE_1[b]	−210.4	(81.0 %)	−229.2	(72.1 %)

[a] The values in parentheses are relative to the attractive interactions $\Delta E_{\text{elstat}} + \Delta E_{\text{orb}}$.
[b] The values in parentheses are relative to the total orbital interactions ΔE_{orb}.

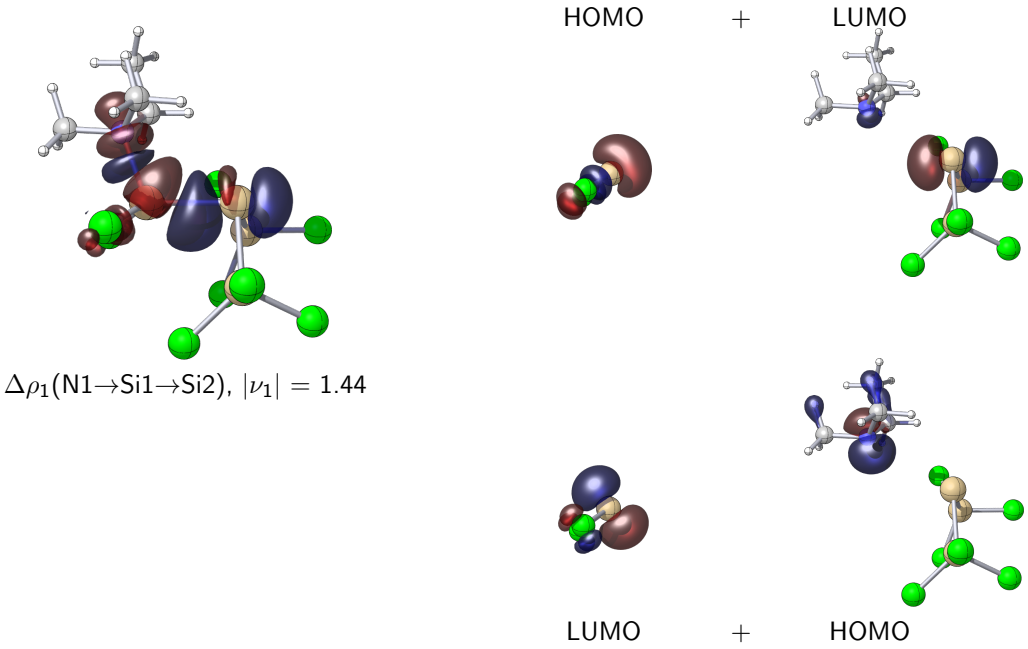

Figure S9. Deformation density $\Delta\rho$ (isocontour 0.005 a_0^{-3}) from EDA-NOCV calculations for the closed-shell N1–Si1–Si2 donor-acceptor interaction in **1** (left). The charge eigenvalues ν quantify the charge transfer between donor and acceptor fragments (in e). The corresponding frontier orbitals (isocontour 0.075 $a_0^{-3/2}$) of the fragments are shown on the right.

Table S14. Energy decomposition analysis of **2** for the Si1–Si2 bonding, relative to the two silylene fragments $SiCl_2$ and $Si(SiCl_3)_2$ (BP86-D/TZ2P//SMD-M06-2X/6-31+G(d,p)). Relative energies are given in kcal mol^{-1}.

Interaction	D/A (Si1→Si2)		shared (Si1··Si2)	
ΔE_{int}	−54.3		−203.0	
ΔE_{disp}	−8.4		−8.4	
ΔE_{pauli}	152.0		158.1	
ΔE_{elstat}[a]	−80.6	(40.7 %)	−170.3	(48.3 %)
ΔE_{orb}[a]	−117.3	(59.3 %)	−182.5	(51.7 %)
ΔE_1[b]	−71.4	(60.8 %)	−114.7	(62.8 %)
ΔE_2[b]	−33.5	(28.5 %)	−43.1	(23.6 %)

[a] The values in parentheses are relative to the attractive intens $\Delta E_{\text{elstat}} + \Delta E_{\text{orb}}$.
[b] The values in parentheses are relative to the total orbital interactions ΔE_{orb}.

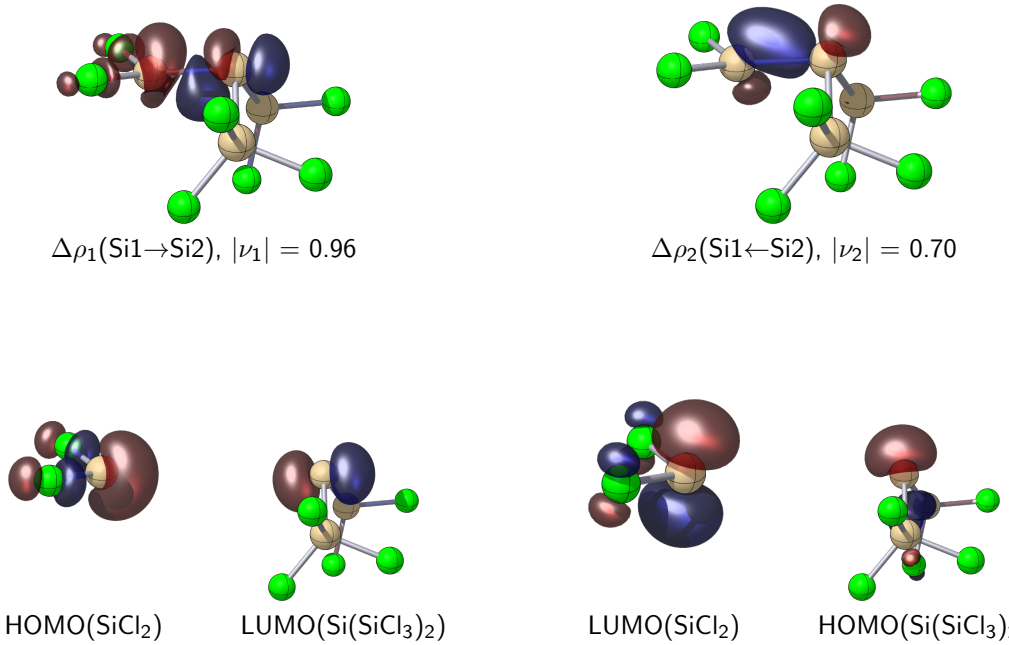

Figure S10. Deformation density $\Delta\rho$ (isocontour 0.005 a_0^{-3}) from EDA-NOCV calculations for the closed-shell Si1–Si2 donor-acceptor interactions in **2** (left). The charge eigenvalues ν quantify the charge transfer between donor and acceptor fragments (in e). The corresponding frontier orbitals (isocontour 0.075 $a_0^{-3/2}$) of the fragments are shown (bottom).

C4. Spin-orbit Relativistic NMR Calculations

The importance of heavy-atom induced spin-orbit effects for nuclear magnetic shifts of group 14 element halides have been stressed by several groups: The experimentally observed normal halogen dependence (NHD, i.e., a characteristic high-field shift of nuclei directly bonded to halogen substituents) increases with the halogen atomic mass[39] and has been attributed to a spin-orbit induced substituent effect. As detailed by Kaupp *et al.*[40] and Autschbach,[41] this effect can be explained in analogy to the relativistic Fermi-contact mechanism of nuclear spin-spin coupling transferred primarily through covalent (σ-) bonds.

In previous work we have noted surprisingly large deviations of computed ^{29}Si NMR chemical shifts from experiment for perchlorinated silanes, which we were able to correct by application of an *ad hoc* correction scheme.[42] Later we realized that these problems were related to the neglect of relativistic spin-orbit effects in our calculations – a somewhat unexpected result in view of the moderate atomic masses involved. However, in keeping with findings of, e.g., Truflandier *et al.*[43] and Chernyshev and Krivdin[44] we recently found that the relativistic SO-ZORA operator as implemented in the ADF program successfully copes with such situations for chlorosilanes.[45] The overall good performance of the PBE0 hybrid functional, used along with the TZ2P Slater basis set, for a representative set of ^{29}Si NMR shift benchmark data comprising five perchlorinated silanes, two $SiCl_2$ base-adducts, as well as three cationic and one anionic species is documented in Table S15.

Table S15. Experimental and calculated NMR chemical shift values of perchlorinated silanes (δ(TMS)=0; ZORA-SO-PBE0(COSMO)/TZ2P//SMD-M06-2X/6-31+G(d,p), solvent toluene).

Compound		Exp. δ(^{29}Si) /ppm	Calc. δ(^{29}Si) /ppm	Δ /ppm
$SiCl_4$[46]		–18.5	–17.6	0.9
Si_2Cl_6[46]		–6.1	–4.2	1.9
Si_3Cl_8[46]	Si^{III}	–3.7	–2.1	1.6
	Si^{II}	–7.4	–7.2	0.2
iso-Si_4Cl_{10}[46]	Si^{III}	0.0	2.1	2.1
	Si^{I}	–31.8	–32.7	–0.9
neo-Si_5Cl_{12}[46]	Si^{III}	4.0	4.7	0.7
	Si^{0}	–80.4	–80.2	0.2
(NHC)$SiCl_2$[47]		19.1	25.8	6.7
($EtMe_2N$)$SiCl_2$[42]		42.7	48.3	5.6
[(NHC)$HSiCl_2$]$^+$[48]		–125.4	–125.4	0.0
[(NHC)$SiCl_3$]$^+$[49]		–20.9	–19.0	1.9
[(NHC)$_2SiCl_3$]$^+$[49]		–110.5	–108.7	1.8
[Si_6Cl_{12}·2Cl]$^{2-}$[50]		–21.7	–18.9	2.8
			MAE	2.0

With a mean absolute down-field shift of 2.0 ppm compared to experiment, larger errors occur for the dichlorosilylene base-adducts (6.2 ppm). For these subvalent species, a pragmatic empirical correction scheme appears useful (the deviation of δ(^{29}Si) of the Si(II) center in **1** profits from a up-field shift of 6.2 ppm compared to experiment, Table S16). In light of the small data set, however, generalization seems inappropriate at this point.

Table S16. Experimental and calculated NMR chemical shift values of perchlorinated silanes. Empirically corrected data (shaded, $\delta(^{29}Si)$calc. –6.2 ppm); δ(TMS)=0; ZORA-SO-PBE0(COSMO)/TZ2P//SMD-M06-2X /6-31+G(d,p), solvent toluene.

Compound		Exp. $\delta(^{29}Si)$ /ppm	Calc. $\delta(^{29}Si)$ /ppm	Corr. $\delta(^{29}Si)$ /ppm	Δ /ppm
$(NHC)SiCl_2$		19.1	25.8	19.6	0.5
$(EtMe_2N)SiCl_2$		42.7	48.3	42.1	–0.6
$(Me_3N)SiCl_2$		–	48.9	42.8	–
1	Si^{II}	43.7	48.7	42.5	–1.2
	Si^{III}	27.9	29.9	–	2.0
	Si^{0}	–155.6	–154.8	–	0.8

Calculated NMR chemical shift values for **1** and the ionic species $[(Me_3N)_2SiCl_3]^+$ and $[Si(SiCl_3)_3]^-$ are in good agreement with the experimentally observed signatures, vindicating the assignment of individual Si atoms (Table S17) and lending weight to the proposed mechanism for the formation of **1** (see section C5).

Table S17. Experimental and calculated NMR chemical shift values for **1** and the ionic intermediates $[(Me_3N)SiCl_3]^+$ and $[Si(SiCl_3)_3]^-$ observed during preparative work (δ(TMS)=0; ZORA-SO-PBE0(COSMO)/ TZ2P//SMD-M06-2X/6-31+G(d,p), solvent toluene).

Compound		Exp. $\delta(^{29}Si)$ /ppm	Calc. $\delta(^{29}Si)$ /ppm	Δ /ppm
1	Si^{II}	43.7	48.7	5.0
	Si^{III}	27.9	29.9	2.0
	Si^{0}	–155.6	–154.8	0.8
$[(Me_3N)SiCl_3]^+$		–	–4.0	–
$[(Me_3N)_2SiCl_3]^+$		–68.8	–67.7	1.1
$[Si(SiCl_3)_3]^-$	Si^{III}	30.9	34.2	3.3
	Si^{0}	–143.1	–137.0	6.1

C5. Additional Information on the Formation Mechanism of 1

As evidenced by low-temperature NMR spectroscopy, compound **1** forms in the course of the amine-induced disproportionation reaction of Si_2Cl_6 and it crystallizes almost quantitatively upon quenching the reaction at –196 °C. Alternatively, it is formed in the reaction of *neo*-Si_5Cl_{12} and amine base, which was again followed by low-temperature NMR spectroscopy. In the latter reaction, efficient formation of **1** was already observed at –70 °C, and its NMR signatures are accompanied by those of the contact ion pair $[(Me_3N)_2SiCl_3]^+[Si(SiCl_3)_3]^-$ as reported above. Here, we present our theoretical investigations on the reaction mechanism in full detail. NMe_3 was used as model base in all calculations.

Initial interaction of the amine and *neo*-Si_5Cl_{12} results in slightly exergonic formation of adduct **A** (Scheme S1). From here, we investigated a number of conceivable pathways for the formation of **1**. Direct elimination of $SiCl_4$ from **A** occurs in a concerted, asynchronous step, which starts with a 1,3-chloride shift followed by a Berry pseudorotation to isomer **f**. Subsequent $SiCl_4$ elimination leads to **1** in an overall thermoneutral reaction. The highest activation barrier along this reaction sequence ($\Delta^{\ddagger}G$ = 22 kcal mol^{-1} for **TSa**, Scheme S2), however, is clearly too high to explain rapid product formation observed at –70 °C.

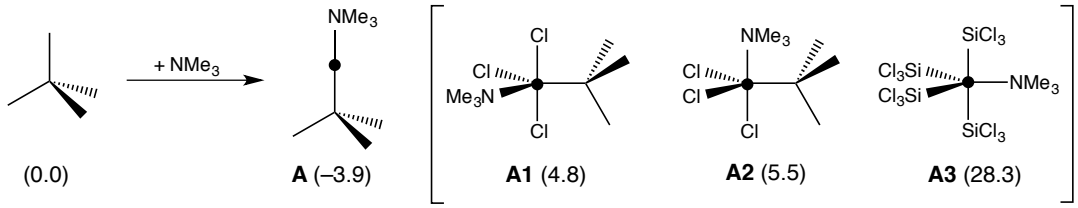

Scheme S1. Initial interaction between neo-Si_5Cl_{12} and amine base (ΔG^{203} in kcal mol^{-1}; SMD-M06-2X/6-311++G(2d,2p)//6-31+G(d,p); solvent toluene).

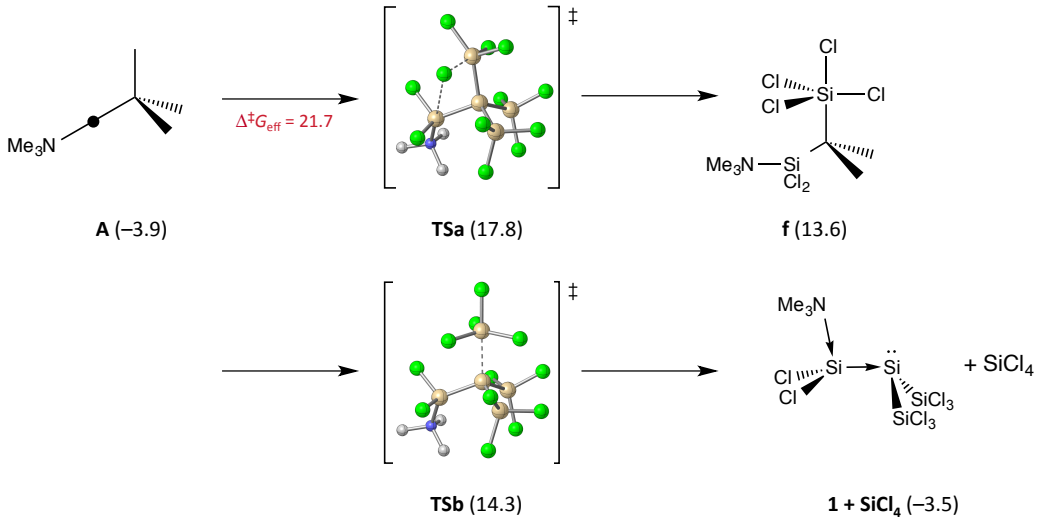

Scheme S2. Base-induced disproportionation reaction of neo-Si_5Cl_{12} to **1** and $SiCl_4$. The rate determining activation barrier is given in red (ΔG^{203} in kcal mol^{-1}; SMD-M06-2X/6-311++G(2d,2p)//6-31+G(d,p); solvent toluene).

The energetically most favored route commences with low-barrier heterolysis of **A** to yield, after coordination of a second amine, the contact ion-pair $[(Me_3N)_2SiCl_3]^+[Si(SiCl_3)_3]^-$ (**B**, Scheme S3) in an overall thermoneutral step. Elimination of the amine-stabilized silyl cation (**TSc**) proceeds

with a moderate barrier of 15 kcal mol^{-1}. Remarkably, the agreement of the ^{29}Si NMR shifts computed for the separate ions with the low-temperature NMR signals ($Si(SiCl_3)_3^-$: 34.2 (–*Si*Cl_3), –137.0 (*Si*($SiCl_3$)$_3$); exp. 30.9, –143.1; $(Me_3N)_2SiCl_3^+$: –67.7; exp. –68.8) allows for a straightforward assignment and lends weight to the relevance of this heterolytic pathway.

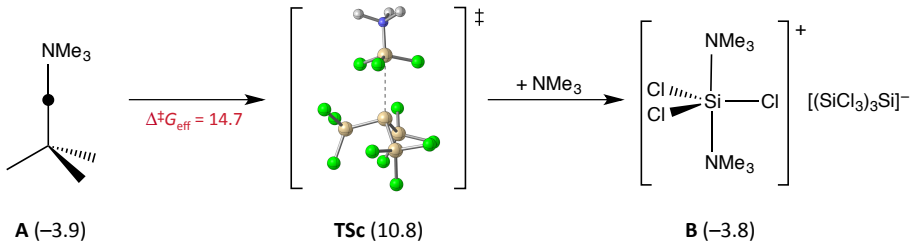

Scheme S3. Heterolysis of neo-Si_5Cl_{12}•NMe_3 to the contact ion pair $[(Me_3N)_2SiCl_3]^+[Si(SiCl_3)_3]^-$. The rate determining activation barrier is given in red (ΔG^{203} in kcal mol^{-1}; SMD-M06-2X/6-311++G(2d,2p)//6-31+G(d,p); solvent toluene).

We investigated two plausible routes for subsequent reactions of the $Si(SiCl_3)_3^-$ anion: First, the $(Me_3N)SiCl_3^+$ cation is liberated as reactive species after dissociation of one NMe_3 molecule from the $(Me_3N)_2SiCl_3^+$ cation. Upon simultaneous *trans*-approach of the liberated amine $(Me_3N)SiCl_3^+$ can abstract a chloride ion from the $Si(SiCl_3)_3^-$ anion (**TSd**, Scheme S4). This thermoneutral reaction is irrelevant at –70 °C, however, owing to the large activation barrier of 26 kcal mol^{-1}.

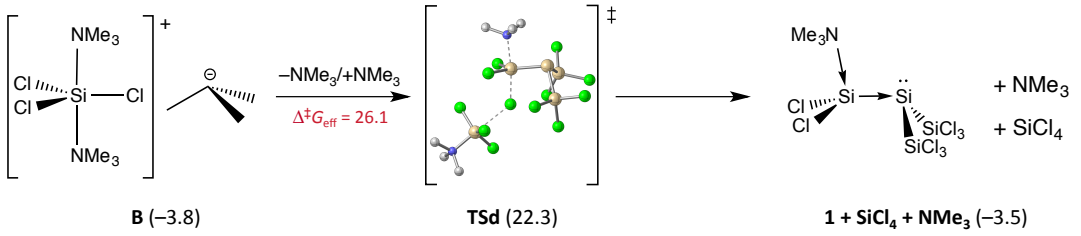

Scheme S4. Chloride abstraction from NMe_3•$Si(SiCl_3)_3^-$ by $(Me_3N)SiCl_3^+$ (ΔG^{203} in kcal mol^{-1}; SMD-M06-2X/6-311++G(2d,2p)//6-31+G(d,p); solvent toluene).

Second, the $Si(SiCl_3)_3^-$ anion can add to *neo*-Si_5Cl_{12} with a minute barrier of 6 kcal mol^{-1} (Scheme S5). Over a sequence of isomerization reactions, akin to pathways reported in related work,[50] the resulting higher silicate **C**$^-$ eliminates $SiCl_4$ in a thermoneutral reaction yielding silanide **E**$^-$. Compound **1** is formed subsequently by S_N2 reaction with NMe_3, liberating again the $Si(SiCl_3)_3^-$ anion. The overall effective barrier for the formation of **1** along this route adds up to 16 kcal mol^{-1} (**TS2** relative to **C**$^-$). Of note, in this scenario the $Si(SiCl_3)_3^-$ anion triggers an autocatalytic reaction. Combined with NMR spectroscopic evidence for the formation of the ions $(Me_3N)_2SiCl_3^+$ and $Si(SiCl_3)_3^-$, this pathway explains the exceptionally high reaction rate.

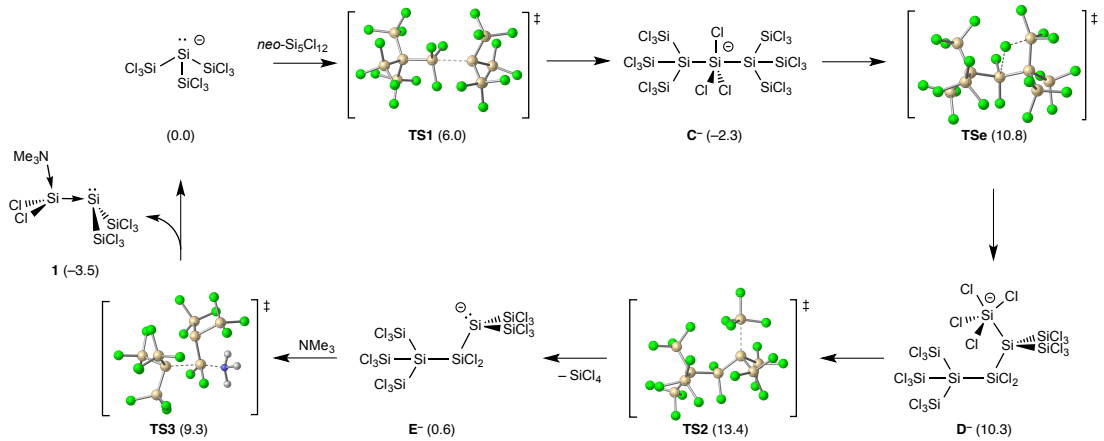

Scheme S5. Catalytic cycle computed for the formation of compound **1** from neo-Si_5Cl_{12} (ΔG^{203} in kcal mol^{-1}; SMD-M06-2X/6-311++G(2d,2p)//6-31+G(d,p); solvent toluene).

In conclusion, the following mechanistic picture for the formation of compound **1** from *neo*-Si_5Cl_{12} and NMe_3 emerges: While the amine-induced disproportionation reaction of *neo*-Si_5Cl_{12}•NMe_3 exhibits a barrier (22 kcal mol^{-1}) too high for effective transformation at –70 °C, heterolysis of the base adduct yielding the contact ion-pair $[(Me_3N)_2SiCl_3]^+[Si(SiCl_3)_3]^-$ represents the energetically most favored route towards formation of **1**. These findings are supported by low-temperature NMR signals for the separated ions, which are assigned according to quantum-chemical calculations.

C6. Comparison of Computed and Experimental Geometry of 1

Table S18. Comparison of selected bond lengths (Å) and angles (°) for the computed and experimental structures of **1**. Geometries are calculated at the SMD-M06-2X/6-31+G(d,p) level of theory (solvent toluene). Experimental data taken from the single-crystal X-ray analysis of the co-crystal **1**•C_6H_6 and of neat **1** from toluene.

bond/angle	calc.	exp.	Δ(calc-exp)	exp.	Δ(calc-exp)
		1•C_6H_6		**1**	
N1–Si1	1.93	1.894(5)	0.04	1.9014(13)	0.03
Si1–Si2	2.34	2.324(2)	0.01	2.3225(6)	0.01
Si2–Si3	2.35	2.310(2)	0.04	2.3090(6)	0.04
Si2–Si4	2.34	2.317(2)	0.03	2.3190(6)	0.02
Si1–Cl1	2.07	2.045(2)	0.03	2.0509(6)	0.02
Si1–Cl2	2.08	2.037(2)	0.04	2.0482(6)	0.03
Si3–Cl3	2.09	2.047(2)	0.04	2.0546(6)	0.03
Si3–Cl4	2.07	2.053(2)	0.02	2.0548(6)	0.02
Si3–Cl5	2.07	2.057(2)	0.02	2.0551(6)	0.02
Si4–Cl6	2.08	2.046(2)	0.03	2.0519(6)	0.02
Si4–Cl7	2.08	2.048(2)	0.03	2.0514(6)	0.02
Si4–Cl8	2.07	2.065(2)	0.01	2.0606(6)	0.01
N1–C1	1.50	1.504(7)	−0.01	1.506(2)	−0.01
N1–C2	1.50	1.503(8)	−0.01	1.505(2)	−0.01
N1–C3	1.52	1.526(7)	−0.01	1.522(2)	−0.01
C3–C4	1.52	1.511(7)	0.01	1.512(2)	0.01
C4–C3–N1	115.4	115.4(5)	0.0	115.42(14)	0.0
C2–N1–C1	108.7	109.2(5)	−0.5	108.63(12)	0.0
C3–N1–C1	110.3	110.3(5)	0.0	110.23(13)	0.1
C3–N1–C2	110.0	109.8(5)	0.2	110.18(13)	−0.2
N1–Si1–Si2	109.1	107.14(15)	2.0	106.98(4)	2.2
Cl1–Si1–Cl2	106.1	105.82(10)	0.3	105.79(3)	0.3
Si1–Si2–Si3	97.4	96.90(8)	0.5	97.63(2)	−0.2
Si1–Si2–Si4	92.8	96.93(8)	−4.1	96.40(2)	−3.6
Si3–Si2–Si4	95.7	97.46(8)	−1.8	99.22(2)	−3.5

C7. Cartesian Coordinates of Optimized Structures

Coordinates in Å; SMD-M06-2X/6-311++G(d,p)//6-31+G(d,p), solvent toluene

28

1 (^{1}A, C_1): E_{tot} = −5053.78020258

Si	−1.952336	−1.283255	−0.325641
Si	−0.250207	0.043969	−1.237672
Si	−0.824744	1.995781	−0.066539
Cl	−3.778302	−0.375049	−0.688808
Cl	−1.974437	−1.781912	1.689764
Cl	−2.009367	−3.104947	−1.321328
Cl	0.811253	3.280419	0.129181
Cl	−2.176220	3.051329	−1.231850
Cl	−1.670239	1.929472	1.821683
Si	1.341853	−0.755720	0.272741
Cl	1.624726	0.037898	2.164293
Cl	1.333679	−2.817274	0.510031
N	3.106597	−0.519917	−0.482068
C	4.187795	−0.979359	0.443807
C	3.260068	0.959886	−0.777153
C	3.196376	−1.307546	−1.752397
H	3.125260	−2.370511	−1.522944
H	2.384445	−1.015143	−2.421076
H	2.497631	1.205173	−1.523012
H	3.018205	1.488973	0.148122
C	4.632802	1.388799	−1.267705
H	5.132042	−1.001554	−0.102547
H	4.261950	−0.293624	1.287432
H	3.954563	−1.983473	0.800287
H	4.157421	−1.108737	−2.227425
H	4.578937	2.461810	−1.469541
H	5.410886	1.236951	−0.516740
H	4.927731	0.899107	−2.198272

12

2 (^{1}A, C_1): E_{tot} = −4839.94523556

Si	−0.038417	0.109874	−1.232521
Si	−1.951104	−0.585179	−0.074549
Si	1.665375	−1.041006	−0.094934
Si	0.299695	2.079993	−0.213796
Cl	−3.428350	0.842727	−0.207353
Cl	−1.722055	−1.048520	1.917864
Cl	−2.658470	−2.278242	−1.002877
Cl	2.076012	−0.557757	1.867633
Cl	3.433346	−0.817570	−1.125376
Cl	1.156083	−3.034163	−0.125716
Cl	−1.012479	3.610870	−0.021220
Cl	2.176050	2.818448	0.027704

12

[**2**]$^{-\cdot}$ (^{2}A, C_1): E_{tot} = -4840.09403119

Si	-0.011994	0.338691	-1.243999
Si	-1.882338	-0.439113	-0.065513
Si	1.473289	-1.130805	-0.179926
Si	0.347009	2.110750	0.296405
Cl	-3.297538	1.093230	0.076176
Cl	-1.754292	-1.179331	1.882145
Cl	-2.863003	-1.958011	-1.108708
Cl	2.004420	-0.905424	1.825322
Cl	3.306974	-1.129601	-1.178326
Cl	0.808634	-3.105419	-0.324250
Cl	-0.556771	3.873730	-0.456931
Cl	2.412546	2.586512	0.267071

16

NMe_2Et (^{1}A, C_1): E_{tot} = -213.74690352

N	0.590102	-0.000001	0.470191
C	1.049445	1.197553	-0.210146
C	1.049440	-1.197555	-0.210146
C	-0.849418	0.000000	0.724072
C	-1.761226	0.000001	-0.507107
H	0.717015	1.261790	-1.261794
H	0.689212	2.085443	0.318829
H	2.143976	1.220066	-0.206602
H	0.717008	-1.261789	-1.261793
H	0.689208	-2.085444	0.318831
H	2.143971	-1.220071	-0.206606
H	-1.071361	0.880670	1.338715
H	-1.071362	-0.880668	1.338717
H	-2.809027	0.000007	-0.190743
H	-1.604400	0.886552	-1.129466
H	-1.604406	-0.886551	-1.129463

16

[NMe_2Et]$^{+\cdot}$ (^{2}A, C_1): E_{tot} = -213.52026466

N	3.522830	-0.486699	-0.733845
C	4.119100	-1.008007	0.470420
C	3.371212	0.943283	-0.920043
C	3.154795	-1.395781	-1.791276
H	3.681771	-2.342455	-1.673139
H	2.070884	-1.570639	-1.726901
H	2.648775	1.105490	-1.721679
H	2.993310	1.363570	0.016395
C	4.737788	1.554214	-1.270641
H	5.126985	-1.374804	0.231935
H	4.173958	-0.234004	1.234270
H	3.526359	-1.860643	0.817616
H	3.371506	-0.937869	-2.759784
H	4.600581	2.625580	-1.429657
H	5.451451	1.412185	-0.455953
H	5.138710	1.112220	-2.185899

9

$Si(SiCl_3)_2$, (^1A, C_1): E_{tot} = -3629.93178624

Si	-0.107756	-1.434821	-0.982256
Si	1.657432	-0.050123	-0.130680
Si	-1.749283	0.030105	-0.261600
Cl	-1.660682	1.847654	0.662267
Cl	-3.678496	-0.249019	-0.880775
Cl	-1.341842	-1.511736	1.227336
Cl	1.588360	0.632860	1.809307
Cl	3.426060	-1.104548	-0.300599
Cl	1.832238	1.585129	-1.387031

9

$[Si(SiCl_3)_2]^{-\cdot}$ (^2B, C_2): E_{tot} = -3630.08537632

Si	0.000000	1.666568	0.226811
Si	0.000000	0.000000	1.862689
Si	0.000000	-1.666568	0.226811
Cl	-1.211013	1.522651	-1.482376
Cl	1.885904	2.166979	-0.556667
Cl	-0.635388	3.482839	1.085268
Cl	0.635388	-3.482839	1.085268
Cl	-1.885904	-2.166979	-0.556667
Cl	1.211013	-1.522651	-1.482376

19

NMe_2Et-$SiCl_2$, (^1A, C_1): E_{tot} = -1423.75430295

Si	-0.876174	0.119621	-0.961381
Cl	-1.211796	1.930139	0.196357
Cl	-2.132727	-1.233129	0.189942
N	0.850192	-0.373106	0.043229
C	0.785911	-0.303792	1.522768
C	1.875771	0.582789	-0.492723
C	1.162556	-1.763802	-0.370531
H	0.369886	-2.427060	-0.020835
H	1.224488	-1.814134	-1.461013
H	1.827185	0.510849	-1.584570
H	1.542251	1.584561	-0.208258
C	3.303077	0.355396	-0.015291
H	1.698360	-0.723237	1.955287
H	0.673256	0.735655	1.832054
H	-0.073113	-0.879219	1.870038
H	2.111284	-2.085688	0.064631
H	3.935120	1.121017	-0.473063
H	3.400051	0.458332	1.068146
H	3.699324	-0.616727	-0.318111

19

$[NMe_2Et\text{-}SiCl_2]^{+\cdot}$, ($^2A$, C_1): E_{tot} = -1423.52933388

Si	-0.833390	0.119628	-0.631869
Cl	-1.235108	1.969473	0.113544
Cl	-2.169980	-1.248940	0.063309
N	0.847971	-0.379102	0.057762
C	0.893103	-0.272208	1.554691
C	1.876093	0.544267	-0.594809
C	1.100228	-1.803943	-0.345946
H	0.415859	-2.459555	0.192469
H	0.953107	-1.910918	-1.423756
H	1.810442	0.353750	-1.670895
H	1.546968	1.568231	-0.398314
C	3.300387	0.361378	-0.100874
H	1.803850	-0.755860	1.910419
H	0.888949	0.778645	1.845729
H	0.028458	-0.785209	1.978955
H	2.125906	-2.064768	-0.086772
H	3.922757	1.064331	-0.660307
H	3.408977	0.603599	0.958080
H	3.694016	-0.639339	-0.288650

17

neo-Si_5Cl_{12}, (^1A, T): E_{tot} = -6970.51717154

Si	0.000000	0.000000	0.000000
Si	-1.345815	1.345815	-1.345815
Cl	-2.005077	2.957047	-0.272394
Cl	-0.272394	2.005077	-2.957047
Cl	-2.957047	0.272394	-2.005077
Si	1.345815	-1.345815	-1.345815
Cl	0.272394	-2.005077	-2.957047
Cl	2.957047	-0.272394	-2.005077
Cl	2.005077	-2.957047	-0.272394
Si	1.345815	1.345815	1.345815
Cl	0.272394	2.005077	2.957047
Cl	2.957047	0.272394	2.005077
Cl	2.005077	2.957047	0.272394
Si	-1.345815	-1.345815	1.345815
Cl	-2.005077	-2.957047	0.272394
Cl	-0.272394	-2.005077	2.957047
Cl	-2.957047	-0.272394	2.005077

5

$SiCl_4$, ($^1A_1$, T_d): E_{tot} = -2130.49304666

Si	0.000000	0.000000	0.000000
Cl	1.172497	1.172497	1.172497
Cl	-1.172497	-1.172497	1.172497
Cl	-1.172497	1.172497	-1.172497
Cl	1.172497	-1.172497	-1.172497

13

NMe_3, ($^1A_1$, C_{3v}): E_{tot} = -174.44101191

N	0.000000	0.000000	0.388999
C	0.000000	1.380396	-0.062741
H	-0.886537	1.895959	0.317885
H	0.000000	1.461598	-1.166989
H	0.886537	1.895959	0.317885
C	-1.195458	-0.690198	-0.062741
H	-2.085217	-0.180216	0.317885
H	-1.198680	-1.715743	0.317885
H	-1.265781	-0.730799	-1.166989
C	1.195458	-0.690198	-0.062741
H	1.265781	-0.730799	-1.166989
H	1.198680	-1.715743	0.317885
H	2.085217	-0.180216	0.317885

30

A, (^1A, C_1): E_{tot} = -7144.98049307

Si	0.321240	-0.000470	-0.000230
Si	1.260210	0.958390	1.914300
Si	1.265740	1.177620	-1.785160
Si	1.260340	-2.138130	-0.125890
Si	-2.090510	0.000870	-0.002410
N	-4.169990	0.001680	-0.001080
C	-4.723580	0.879820	1.076530
H	-4.260390	1.864980	1.033570
H	-4.544900	0.428820	2.050530
H	-5.800730	0.980340	0.917810
C	-4.726750	0.495810	-1.299040
H	-4.269130	-0.037540	-2.131740
H	-4.544770	1.564180	-1.397430
H	-5.804680	0.311460	-1.302250
C	-4.725980	-1.369640	0.221000
H	-4.552800	-1.986960	-0.658250
H	-5.802310	-1.280320	0.392150
H	-4.260650	-1.827240	1.093290
Cl	-2.124640	-0.597470	2.023020
Cl	-2.126110	2.052840	-0.499890
Cl	-2.126500	-1.453340	-1.532310
Cl	0.150090	-3.484480	0.963040
Cl	3.179800	-2.177220	0.610620
Cl	1.334510	-2.811360	-2.068330
Cl	0.159150	0.910140	-3.498430
Cl	3.185120	0.556090	-2.182810
Cl	1.342850	3.196320	-1.397060
Cl	0.147340	2.572590	2.536700
Cl	3.177890	1.620020	1.577160
Cl	1.338720	-0.386550	3.468890

43

B, (^{1}A, C_1): E_{tot} = -7319.43982784

Si	-0.866686	-0.109396	0.177959
Si	-1.752507	0.493069	-1.889903
Si	-1.956641	1.528445	1.420649
Si	-2.347542	-1.851032	0.618531
Si	3.378365	-0.117747	0.020849
N	3.339670	1.947595	0.017333
C	3.852672	2.518633	-1.268997
H	3.129599	2.352159	-2.064849
H	4.807811	2.062665	-1.529976
H	3.992312	3.594162	-1.134825
C	1.943269	2.466630	0.197270
H	1.591665	2.251346	1.205754
H	1.278568	2.012952	-0.539026
H	1.958115	3.549123	0.043789
C	4.174142	2.531831	1.114027
H	3.904724	2.090032	2.072115
H	3.983755	3.607631	1.152180
H	5.229700	2.361838	0.907407
Cl	5.452731	-0.102412	-0.083254
Cl	2.336928	-0.127477	-1.762066
Cl	2.517454	-0.122389	1.899798
Cl	-2.563241	-2.076879	2.677495
Cl	-1.476818	-3.645574	-0.018198
Cl	-4.268921	-1.920577	-0.155656
Cl	-1.133478	1.608144	3.337847
Cl	-4.005263	1.531740	1.732234
Cl	-1.516156	3.399314	0.595683
Cl	-0.521254	1.926356	-2.795965
Cl	-3.660487	1.270683	-2.120260
Cl	-1.653672	-1.154830	-3.163788
N	3.371537	-2.184712	0.025945
C	4.038938	-2.747177	1.242245
H	5.015952	-2.284904	1.383128
H	4.169415	-3.822311	1.096210
H	3.417491	-2.580140	2.119215
C	4.082112	-2.758217	-1.159886
H	5.149561	-2.555023	-1.087815
H	3.682459	-2.337886	-2.081242
H	3.921179	-3.839444	-1.163162
C	1.970536	-2.721786	0.004609
H	2.016028	-3.805480	0.143098
H	1.499480	-2.501034	-0.952436
H	1.387956	-2.278432	0.811979

25

1′ (^{1}A, C_1): E_{tot} = -5014.47354991

Si	-1.483318	-1.622989	-0.207573
Si	-0.181232	0.005343	-1.272899
Si	-1.106143	1.839107	-0.138979
Cl	-3.482918	-1.166188	-0.496076
Cl	-1.289738	-2.004818	1.823902
Cl	-1.172431	-3.460573	-1.123005
Cl	0.244443	3.430802	-0.076583
Cl	-2.697011	2.542282	-1.266429
Cl	-1.834579	1.682812	1.791534
Si	1.629550	-0.331153	0.161132
Cl	1.843344	0.644259	1.973677
Cl	2.116906	-2.318239	0.505435
N	3.244165	0.230779	-0.737713
C	4.473150	0.085055	0.102047
C	3.097984	1.669410	-1.121908
C	3.422181	-0.577313	-1.986736
H	3.651863	-1.609310	-1.722868
H	2.507485	-0.537756	-2.581083
H	2.256301	1.778692	-1.809251
H	2.935054	2.272561	-0.227778
H	4.017612	1.987619	-1.618966
H	5.337403	0.343114	-0.515094
H	4.416083	0.760169	0.955133
H	4.560563	-0.945966	0.445971
H	4.248337	-0.147506	-2.557788

13

iso-$Si_4Cl_9^-$, (^{1}A, C_1): E_{tot} = -5300.39248519

Si	1.100209	0.285908	-0.801409
Si	-0.022222	-1.762672	-0.938483
Cl	1.096970	-3.238006	0.025657
Cl	-1.967707	-2.044905	-0.250582
Cl	-0.112830	-2.393461	-2.926768
Si	-0.841496	1.589755	-0.883468
Cl	-1.930952	1.116413	-2.600534
Cl	-2.255119	1.615034	0.645437
Cl	-0.341538	3.602771	-1.122776
Si	1.258630	0.278752	1.533778
Cl	3.102998	-0.509150	2.116189
Cl	1.282099	2.238956	2.252460
Cl	-0.105197	-0.710265	2.758220

30

C^{-}, (^{1}A, C_1): E_{tot} = -12270.92893440

Si	0.003580	-0.004015	-0.006110
Si	0.768824	-1.023067	2.034723
Si	-0.764992	1.024939	-2.040353
Si	-0.649481	-0.369233	-3.915861
Si	0.433000	2.939196	-2.653302
Si	-2.996201	1.727008	-1.967469
Cl	-0.583083	0.709902	-5.674380
Cl	-2.284275	-1.614450	-4.054389
Cl	1.034412	-1.546274	-3.861657
Cl	0.960177	4.043032	-1.002176
Cl	2.157966	2.479001	-3.680142
Cl	-0.670053	4.174944	-3.885157
Cl	-3.819444	1.883249	-3.853872
Cl	-4.152881	0.397403	-0.910645
Cl	-3.197323	3.576944	-1.084779
Si	-0.870845	-2.251418	3.164489
Si	1.555164	0.501012	3.626370
Si	2.526787	-2.540129	1.747706
Cl	-0.984998	1.534849	1.137914
Cl	-1.063639	-4.159930	2.414338
Cl	-2.706330	-1.336511	3.033435
Cl	-0.428766	-2.452012	5.170911
Cl	0.028243	1.308837	4.748114
Cl	2.858225	-0.383046	4.961217
Cl	2.564723	2.051644	2.731699
Cl	2.633316	-3.893856	3.302464
Cl	2.291666	-3.622463	0.016745
Cl	4.357296	-1.600814	1.660485
Cl	2.045975	0.260908	-0.642893
Cl	-1.046013	-1.814892	-0.519156

30

D^{-}, (^{1}A, C_1): E_{tot} = -12270.91001660

Si	2.076474	0.065922	-0.101821
Si	2.714303	0.417406	2.134188
Si	3.651217	1.412596	-1.259308
Si	2.632676	-2.159518	-0.627738
Si	-0.071229	0.852435	-0.767200
Si	-2.167572	0.049597	-0.040014
Si	-3.631501	0.972661	-1.631102
Si	-2.296233	-2.380591	0.205409
Si	-2.693315	1.285534	1.877119
Cl	1.396607	-3.557020	0.187786
Cl	2.625350	-2.329267	-2.673170
Cl	4.518395	-2.616312	0.049772
Cl	5.435087	0.419802	-1.498046
Cl	3.059183	2.004224	-3.127484
Cl	4.040919	3.119064	-0.181422
Cl	2.202036	2.255187	2.869660
Cl	4.767812	0.300213	2.235892
Cl	1.950688	-1.038350	3.352501
Cl	0.173571	2.885756	-0.370014
Cl	-0.075076	0.622647	-2.832644
Cl	-4.408372	-2.245165	0.219248
Cl	-2.303115	-4.526753	0.467365
Cl	-1.342234	-2.527672	-1.695146
Cl	-1.088976	1.408173	3.167234
Cl	-3.241832	3.233389	1.459650
Cl	-4.247772	0.438626	2.926813
Cl	-5.504911	1.230269	-0.797479
Cl	-3.054317	2.828833	-2.329530
Cl	-3.878034	-0.232311	-3.280444
Cl	-1.201920	-2.098308	2.022782

25

E^{-}, (^{1}A, C_1): E_{tot} = -10140.41737230

Si	-1.646693	0.013348	0.040038
Si	-2.419157	2.201265	-0.198163
Si	-3.170371	-1.086169	1.440098
Si	-1.935841	-0.945502	-2.073448
Si	0.579028	-0.332940	0.791926
Si	2.114765	0.010553	-0.954358
Si	3.635519	-1.609283	-0.216004
Si	3.276535	1.818170	-0.014178
Cl	-1.394582	0.377245	-3.548842
Cl	-0.813574	-2.645440	-2.285376
Cl	-3.908012	-1.444720	-2.396838
Cl	-5.065672	-0.295822	1.282932
Cl	-3.305641	-3.083030	0.973924
Cl	-2.611935	-0.921902	3.406460
Cl	-2.771868	3.018644	1.653145
Cl	-4.176135	2.248786	-1.268151
Cl	-1.081065	3.381674	-1.197774
Cl	0.704156	0.704765	2.598412
Cl	0.363569	-2.357562	1.309490
Cl	2.013593	3.422181	0.393269
Cl	4.439902	1.628574	1.700573
Cl	4.603647	2.551465	-1.445945
Cl	5.532748	-1.159774	-0.954110
Cl	3.950622	-2.021772	1.800242
Cl	3.163012	-3.460501	-1.046278

30

TS1, (^{1}A, C_1): E_{tot} = -12270.91216770

Si	-0.506923	-0.052930	-0.061802
Si	2.648604	0.023013	0.396177
Si	-2.835236	-0.076904	-0.407097
Si	-3.995108	0.750708	1.440912
Si	-3.642430	-2.228460	-0.812099
Si	-3.451631	1.240923	-2.231248
Cl	-5.951769	0.122299	1.407100
Cl	-3.990990	2.802311	1.436165
Cl	-3.144381	0.096599	3.185419
Cl	-2.335786	-3.282791	-1.985278
Cl	-3.907048	-3.243712	0.951535
Cl	-5.454424	-2.156428	-1.778914
Cl	-5.428956	1.784325	-2.093339
Cl	-2.321987	2.947368	-2.301789
Cl	-3.200135	0.214694	-3.990182
Si	3.706820	2.065167	0.035274
Si	4.026888	-1.329000	-0.904869
Si	3.526180	-0.476931	2.493268
Cl	0.176035	-0.139908	-2.002104
Cl	3.421275	3.331805	1.661053
Cl	2.808501	3.031962	-1.574207
Cl	5.741987	2.142846	-0.373936
Cl	4.244582	-0.522834	-2.810618
Cl	5.952554	-1.788884	-0.275938
Cl	3.111441	-3.175442	-1.193261
Cl	5.424679	0.174822	3.029485
Cl	2.272147	0.273005	3.974648
Cl	3.548014	-2.537235	2.787445
Cl	-0.249498	-1.750833	1.072590
Cl	-0.285670	1.745551	0.916525

30

TS2, (^{1}A, C_1): E_{tot} = -12270.90470510

Si	-2.169502	0.018877	-0.087949
Si	-2.879717	-0.142553	2.140735
Si	-3.854782	-1.168726	-1.236302
Si	-2.447440	2.266317	-0.683245
Si	-0.074597	-0.920258	-0.713161
Si	2.055435	-0.203464	-0.025695
Si	3.320723	-1.501951	-1.518588
Si	3.043494	2.543110	0.080120
Si	2.365801	-1.459520	1.910093
Cl	-0.890012	3.401792	0.000210
Cl	-2.546284	2.432500	-2.726702
Cl	-4.160307	3.077572	0.108817
Cl	-5.495537	0.041246	-1.528285
Cl	-3.296726	-1.865009	-3.077771
Cl	-4.474425	-2.785612	-0.128446
Cl	-2.526082	-1.971870	2.982141
Cl	-4.915806	0.155940	2.219443
Cl	-2.005579	1.326551	3.275420
Cl	-0.593595	-2.929801	-0.434313
Cl	-0.077692	-0.537347	-2.770496
Cl	4.857978	1.560006	0.080415
Cl	3.753053	4.526293	0.172509
Cl	2.070326	2.671300	-1.736374
Cl	0.795375	-1.065306	3.212657
Cl	2.478993	-3.524192	1.771962
Cl	4.079606	-0.877310	2.916153
Cl	5.098429	-2.088600	-0.617230
Cl	2.511785	-3.244293	-2.299500
Cl	3.875101	-0.380408	-3.171242
Cl	1.988941	2.544451	1.860979

38

TS3, (^{1}A, C_1): E_{tot} = -10314.86270030

Si	1.633933	-0.068268	0.021636
Si	1.903797	0.172076	-2.289340
Si	3.562564	-1.330151	0.476036
Si	2.393057	2.038149	0.672472
Si	-0.770356	-1.387811	1.023327
Si	-1.630747	0.250603	-0.502543
Si	-2.678018	1.800453	0.947739
Si	-3.648970	-0.497436	-1.479934
Cl	0.868971	3.432650	0.555556
Cl	2.986354	1.981351	2.663460
Cl	3.969181	2.906255	-0.362158
Cl	5.421959	-0.404840	0.460424
Cl	3.438731	-2.190230	2.366333
Cl	3.741882	-2.937438	-0.832706
Cl	0.877420	-1.323501	-3.295045
Cl	3.842273	0.096144	-3.036874
Cl	1.135618	1.969361	-2.977771
Cl	0.189167	-3.058263	0.188950
Cl	0.036824	-0.898204	2.892021
Cl	-4.378385	1.135356	-2.540803
Cl	-3.180436	-1.952958	-2.903116
Cl	-5.377754	-1.300613	-0.581325
Cl	-2.725387	3.637015	-0.022103
Cl	-4.673710	1.551232	1.552768
Cl	-1.688967	2.133488	2.745391
N	-2.216188	-2.543526	1.853119
C	-1.730899	-3.447945	2.937116
H	-2.529456	-4.156930	3.175235
H	-1.486317	-2.864986	3.822556
H	-0.848071	-3.990358	2.595700
C	-2.849528	-3.402240	0.810801
H	-3.829258	-3.731529	1.167255
H	-2.214474	-4.264802	0.616178
H	-2.977347	-2.845066	-0.116914
C	-3.253635	-1.641433	2.426997
H	-3.991078	-2.243294	2.966768
H	-3.756917	-1.106888	1.622828
H	-2.786678	-0.934044	3.116518

References

[1] W. Molnar, A. Lugstein, T. Wojcik, P. Pongratz, N. Auner, C. Bauch, E. Bertagnolli, *Beilstein J. Nanotechnol.* **2012**, *3*, 564-569.

[2] A. Kaczmarczyk, G. Urry, *J. Am. Chem. Soc.* **1960**, *82*, 751-752.

[3] G. Urry, *Acc. Chem. Res.* **1970**, *3*, 306-312.

[4] I. M. Alecu, J. Zheng, Y. Zhao, D. G. Truhlar, *J. Chem. Theor. Comput.* **2010**, *6*, 2872-2887.

[5] APEX2 v2014.9-0 (SAINT/SADABS/SHELXT/SHELXL), Bruker AXS Inc., Madison, WI, USA, **2014**.

[6] M. J. Frisch, G. W. Trucks, H. B. Schlegel, G. E. Scuseria, M. A. Robb, J. R. Cheeseman, G. Scalmani, V. Barone, B. Mennucci, G. A. Petersson, H. Nakatsuji, M. Caricato, X. Li, H. P. Hratchian, A. F. Izmaylov, J. Bloino, G. Zheng, J. L. Sonnenberg, M. Hada, M. Ehara, K. Toyota, R. Fukuda, J. Hasegawa, M. Ishida, T. Nakajima, Y. Honda, O. Kitao, H. Nakai, T. Vreven, J. A. Montgomery, Jr., J. E. Peralta, F. Ogliaro, M. Bearpark, J. J. Heyd, E. Brothers, K. N. Kudin, V. N. Staroverov, R. Kobayashi, J. Normand, K. Raghavachari, A. Rendell, J. C. Burant, S. S. Iyengar, J. Tomasi, M. Cossi, N. Rega, J. M. Millam, M. Klene, J. E. Knox, J. B. Cross, V. Bakken, C. Adamo, J. Jaramillo, R. Gomperts, R. E. Stratmann, O. Yazyev, A. J. Austin, R. Cammi, C. Pomelli, J. W. Ochterski, R. L. Martin, K. Morokuma, V. G. Zakrzewski, G. A. Voth, P. Salvador, J. J. Dannenberg, S. Dapprich, A. D. Daniels, O. Farkas, J. B. Foresman, J. V. Ortiz, J. Cioslowski, D. J. Fox, Gaussian 09, Revision D.01, Gaussian, Inc., Wallingford CT, **2009**.

[7] Y. Zhao, D. Truhlar, *Theor. Chem. Acc.* **2008**, *120*, 215-241.

[8] R. Ditchfield, W. J. Hehre, J. A. Pople, *J. Chem. Phys.* **1971**, *54*, 724-728.

[9] A. V. Marenich, C. J. Cramer, D. G. Truhlar, *J. Chem. Phys. B* **2009**, *113*, 6378-6396.

[10] S. E. Wheeler, K. N. Houk, *J. Chem. Theor. Comput.* **2010**, *6*, 395-404.

[11] A. D. McLean, G. S. Chandler, *J. Chem. Phys.* **1980**, *72*, 5639-5648.

[12] R. Krishnan, J. S. Binkley, R. Seeger, J. A. Pople, *J. Chem. Phys.* **1980**, *72*, 650-654.

[13] E. D. Glendening, J. K. Badenhoop, A. E. Reed, J. E. Carpenter, J. A. Bohmann, C. M. Morales, C. R. Landis, F. Weinhold, NBO 6.0, Theoretical Chemistry Institute, University of Wisconsin, Madison, **2013**.

[14] E. D. Glendening, C. R. Landis, F. Weinhold, *WIREs Comput. Mol. Sci.* **2012**, *2*, 1-42.

[15] E. D. Glendening, C. R. Landis, F. Weinhold, *J. Comput. Chem.* **2013**, *34*, 1429-1437.

[16] T. Lu, Multiwfn 3.3.7 - A Multifunctional Wavefunction Analyzer, School of Chemical and Biological Engineering, University of Science and Technology, Beijing, China, **2013**.

[17] T. Lu, F. Chen, *J. Comput. Chem.* **2012**, *33*, 580-592.

[18] R. F. W. Bader, *Atoms in Molecules: A Quantum Theory*, Oxford University Press, Oxford, **1990**.

[19] *The Quantum Theory of Atoms in Molecules* (Eds.: C. F. Matta, R. J. Boyd), Wiley-VCH, Weinheim, **2007.**

[20] O. A. Zhikol, A. F. Oshkalo, O. V. Shishkin, O. V. Prezhdo, *Chem. Phys.* **2003**, *288*, 159-169.

[21] G. Schreckenbach, T. Ziegler, *J. Phys. Chem.* **1995**, *99*, 606-611.

[22] M. Krykunov, T. Ziegler, E. v. Lenthe, *Int. J. Quantum Chem.* **2009**, *109*, 1676-1683.

[23] ADF2014, SCM, Theoretical Chemistry, Vrije Universiteit, Amsterdam, The Netherlands, http://www.scm.com, **2014**.

[24] G. te Velde, F. M. Bickelhaupt, E. J. Baerends, C. Fonseca Guerra, S. J. A. van Gisbergen, J. G. Snijders, T. Ziegler, *J. Comput. Chem.* **2001**, *22*, 931-967.

[25] E. van Lenthe, E. J. Baerends, J. G. Snijders, *J. Chem. Phys.* **1993**, *99*, 4597-4610.

[26] E. van Lenthe, E. J. Baerends, J. G. Snijders, *J. Chem. Phys.* **1994**, *101*, 9783-9792.

[27] E. van Lenthe, J. G. Snijders, E. J. Baerends, *J. Chem. Phys.* **1996**, *105*, 6505-6516.

[28] S. K. Wolff, T. Ziegler, E. van Lenthe, E. J. Baerends, *J. Chem. Phys.* **1999**, *110*, 7689-7698.

[29] J. P. Perdew, K. Burke, M. Ernzerhof, *Phys. Rev. Lett.* **1996**, *77*, 3865-3868.

[30] J. P. Perdew, K. Burke, M. Ernzerhof, *Phys. Rev. Lett.* **1997**, *78*, 1396-1396.

[31] C. Adamo, V. Barone, *J. Chem. Phys.* **1999**, *110*, 6158-6170.

[32] E. van Lenthe, E. J. Baerends, *J. Comput. Chem.* **2003**, *24*, 1142-1156.

[33] A. Klamt, G. Schüürmann, *J. Chem. Soc., Perkin Trans. 2* **1993**, *5*, 799-805.

[34] C. C. Pye, T. Ziegler, *Theor. Chem. Acc.* **1999**, *101*, 396-408.

[35] M. P. Mitoraj, A. Michalak, T. Ziegler, *J. Chem. Theor. Comput.* **2009**, *5*, 962-975.

[36] M. Mitoraj, A. Michalak, *Organometallics* **2007**, *26*, 6576-6580.

[37] C. Y. Legault, Cylview 1.0b, Université de Sherbrooke, http://www.cylview.org, **2009**.

[38] G. A. Andrienko, ChemCraft, http://www.chemcraftprog.com, **2015**.
[39] J. Autschbach, S. Zheng, *Ann. Rep. NMR Spectrosc.* **2009**, *67*, 1-95.
[40] M. Kaupp, O. L. Malkina, V. G. Malkin, P. Pyykkö, *Chem. Eur. J.* **1998**, *4*, 118-126.
[41] J. Autschbach in *Science and Technology of Atomic, Molecular, Condensed Matter & Biological Systems* (Ed. H. C. Rubén), Elsevier, **2013**, pp. 69-117.
[42] F. Meyer-Wegner, A. Nadj, M. Bolte, N. Auner, M. Wagner, M. C. Holthausen, H.-W. Lerner, *Chem. Eur. J.* **2011**, *17*, 4715-4719.
[43] L. A. Truflandier, E. Brendler, J. Wagler, J. Autschbach, *Angew. Chem.* **2011**, *123*, 269-273.
[44] K. A. Chernyshev, L. B. Krivdin, *Russ. J. Org. Chem.* **2012**, *48*, 1518-1525.
[45] C. Zhang, P. Patschinski, D. S. Stephenson, R. Panisch, J. H. Wender, M. C. Holthausen, H. Zipse, *Phys. Chem. Chem. Phys.* **2014**, *16*, 16642-16650.
[46] H. C. Marsmann, W. Raml, E. Hengge, *Z. Naturforsch. B* **1980**, *35*, 35-37.
[47] R. S. Ghadwal, H. W. Roesky, S. Merkel, J. Henn, D. Stalke, *Angew. Chem. Int. Ed.* **2009**, *48*, 5683-5686.
[48] T. Böttcher, S. Steinhauer, B. Neumann, H. G. Stammler, G. V. Röschenthaler, B. Hoge, *Chem. Commun.* **2014**, *50*, 6204-6206.
[49] T. Böttcher, S. Steinhauer, L. C. Lewis-Alleyne, B. Neumann, H. G. Stammler, B. S. Bassil, G. V. Röschenthaler, B. Hoge, *Chem. Eur. J.* **2015**, *21*, 893-899.
[50] J. Tillmann, L. Meyer, J. I. Schweizer, M. Bolte, H.-W. Lerner, M. Wagner, M. C. Holthausen, *Chem. Eur. J.* **2014**, *20*, 9234-9239.